Low Fouling and Biodegradable Protein-Based Particles for Thrombus Imaging

Thomas Bonnard[†], Anand Jayapadman[†], Jasmine A. Putri[†], Jiwei Cui[§‡], Yi Ju[§], Catherine Carmichael[#], Thomas A. Angelovich[¥], Stephen H. Cody[ǂ], Shauna French[⌘], Karline Pascaud[†], Hannah A. Pearce[†], Shweta Jagdale[†], Frank Caruso[§], Christoph E. Hagemeyer[†]*

[†]Nanobiotechnology Laboratory, Australian Centre for Blood Diseases, Central Clinical School, Monash University, Melbourne 3004, Victoria, Australia.

[§]ARC Centre of Excellence in Convergent Bio-Nano Science and Technology, and the Department of Chemical Engineering, The University of Melbourne, Parkville, Victoria 3010, Australia.

[‡]Key Laboratory of Colloid and Interface Chemistry of the Ministry of Education, and the School of Chemistry and Chemical Engineering, Shandong University, Jinan 250100, China.

[#]Mammalian Functional Genetics Laboratory, Australian Centre for Blood Diseases, Central Clinical School, Monash University, Melbourne 3004, Victoria, Australia.

[¥]Chronic Infectious and Inflammatory Diseases Program, School of Health and Biomedical Sciences, RMIT University, Melbourne, Australia and Life Sciences, Burnet Institute, Melbourne, Australia.

[ǂ]Monash Micro Imaging, Monash University, Melbourne 3004, Victoria, Australia.

[⌘] Platelets and Thrombosis Laboratory, Australian Centre for Blood Diseases, Central Clinical School, Monash University, Melbourne 3004, Victoria, Australia.

*Send email correspondence to christoph.hagemeyer@monash.edu

ABSTRACT:

Nanomedicine holds great promise for vascular disease diagnosis and specific therapy, yet rapid sequestration by the mononuclear phagocytic system is limiting the efficacy of particle-based agents. The use of low fouling polymers, such as poly(ethylene glycol), efficiently reduces this immune recognition but these non-degradable polymers can accumulate in the human body and may cause adverse effects after prolonged use. Thus, new particle formulations combining stealth and biocompatible features are required to enable clinical use. Here, a low fouling particle platform is described using exclusively protein material. A recombinant protein with superior hydrophilic characteristics provided by the amino acid repeat proline, alanine, and serine (PAS) is designed and crosslinked into particles with lysine (K) and polyglutamic acid (E) using mesoporous silica templating. The obtained PASKE particles have low fouling behavior, a prolonged circulation time compared to albumin-based particles and are rapidly degraded in the cell's lysosomal compartment. When labelled with near-infrared fluorescent molecules and functionalized with an anti Glycoprotein IIb/IIIa single-chain antibody targeting activated platelets, the particles show potential as a non-invasive molecular imaging tool in a mouse model of carotid artery thrombosis. The PASKE particles constitute a promising biodegradable and versatile platform for molecular imaging of vascular diseases.

KEYWORDS: Protein particles, Biodegradability, Low fouling, Clearance, Thrombosis, Near-infrared imaging

The translation of nanomedicine is challenged by the complex interaction with human physiology and the difficulty to design injectable materials combining low toxicity with all the required features for efficient accumulation at the disease sites.[1, 2, 3] Unlike soluble small molecules, particle-based agents are approximately the size of cellular structures and are easily recognized by the host as pathogens. When entering the blood, various proteins referred to as opsonins are non-specifically adsorbed onto the surface of particles, forming a protein corona, which promotes sequestration by cells of the mononuclear phagocytic system (MPS).[4, 5] This causes rapid blood clearance which in turn dramatically reduces the amount of injected material that reaches the intended target sites.[6]

The main strategy to overcome fast blood clearance is to design "stealth" particles, often achieved by introducing low fouling materials that limit opsonization.[7] The coating of injectable carriers with highly hydrophilic and neutral polymers reduces nonpolar and electrostatic interactions with hydrophobic surfaces and charged biomolecule domains.[8] This technique has been extensively applied with polymers such as Polyethylene glycol (PEG) and has successfully improved the bioavailability of various nanomaterials,[9, 10, 11, 12] including a range of pharmaceuticals that are used clinically.[13] Yet, intravenous administration of PEGylated compounds raises several concerns: adverse immunological responses have been reported; oxidative damage in biological milieus may occur; and non-biodegradable polymers may accumulate in lysosomes causing cytoplasm vacuolation and cell dysfunction in the long term.[14, 15, 16] Moreover, the advantages of avoiding MPS clearance seems to be offset by the adaptive immune system with the generation of anti-PEG immunoglobulin M (IgM), which can result in a drastic acceleration of blood clearance of the injected materials upon subsequent injections.[17, 18]

These limitations have driven efforts to discover alternate low biofouling materials.[8, 14, 19] Among the options considered, protein-based materials are of specific interest because they solve the problem of non-biodegradability.[14] Thus, several methods have been attempted with homo-polymers of small uncharged amino acids such as poly(hydroxyethyl-L-asparagine), poly(hydroxyethyl-L-glutamine) or glycine-rich homo polymer, which provided encouraging low fouling features.[15, 20] More recently, Schlapshy *et al.* significantly improved this approach and reported that sequences comprising repeats of the three amino acids Proline (P), Alanine (A) and Serine (S) result in the biosynthesis of long hydrophilic and highly soluble polypeptide chains exhibiting properties similar to PEG.[21] This so-called PASylation strategy has now been applied to a range of biomolecules, efficiently prolonging the circulation time from 10 to 100 times.[21, 22, 23, 24]

Biodegradability is a required feature for particles that are too large to be excreted from the blood *via* renal clearance (>10nm), as their accumulation in tissue has raised long-term toxicity concerns.[25, 26, 27] Accumulation of non-degradable particles in MPS cells might saturate lysosomes and perturb their degradative and autophagic pathways.[28] When considering that this off-target sequestration is ultimately relevant for the majority of injected particles, it is absolutely essential to allow their timely degradation and elimination from the cells.[29, 30] In this context, using protein as the building block material for the assembly of particle-based agents appears favorable if the lysosomal proteases enable degradation of the particles into small amino acid oligomers which can be metabolized and recycled by physiological pathways.[31]

Here, we exclusively use protein material to produce, *via* mesoporous silica (MS) template technology, particles that combine rapid biodegradation in the lysosomal cell compartment with stealth properties provided by the hydrophilicity of the proline, alanine and serine (PAS) residues.

To ensure full biodegradability, we crosslinked the PASK building blocks with poly(L-glutamic acid) (PGA) (E), a homo amino acid polymer often used for its biocompatibility and degradability by lysosomal proteases.[32, 33, 34] We further assessed the capacities of the obtained PASKE particles as a non-invasive molecular imaging tool of thrombosis and we tested their capacities to cross an inflamed endothelium.

RESULTS AND DISCUSSION

Synthesis and characterization of the PASKE particles. We recombinantly produced a 37.8 kDa protein building block composed of random repeats of proline, alanine and serine amino acids, introducing lysine residues every 20 amino acids for crosslinking purposes and a polyhistidine tag at the C-terminus for purification (Figure 1A). The so-called PASK protein was produced in *E. coli*, purified and identified by sodium dodecyl sulfate (SDS) gel electrophoresis and western blot anti-his-HRP at a size of approximatively 100 kDa (Figure 1B). The important difference to the calculated size is in line with previous studies reporting PASylated proteins and is attributed to reduced binding of SDS to the highly hydrophilic PASK protein, resulting in diminished electrophoresis mobility.[21, 24] To reduce batch-to-batch variations during nanoparticle assembly we only used highly purified PASK protein building blocks with over 95% purity based on the SDS gel electrophoresis analysis. Starting material of lower purity led to significant batch-to-batch variations or no particles were formed. The isolated PASK building blocks were assembled into particles using the previously described mesoporous silica (MS) template technology (Figure 1C).[35, 36, 37] Well-dispersed PASKE particles of ~730-nm diameter were obtained after dissolution of the ~1200-nm MS template using buffered hydrofluoric acid (Figure 1D and E). We have previously shown that the mesoporous template technology enables the generation of well-defined

particle sizes within the sub micrometer range down to 100-150 nm.[35] We recently confirmed that this method was also efficient using peptide material as building blocks.[38] It should be noted that in this study we used 8-Arm-poly(ethylene glycol)-thiol brushes to crosslink the peptide building blocks. For the synthesis of the herein described PASKE particles, we replaced the PEG based crosslinker with poly(L-glutamic acid) (PGA), thereby using exclusively protein material. In contrast to the PEG linked and peptides based particles described by Suma *et al.* that increased in size after template removal (final diameter of ~185 nm using ~135 nm templates), the PASKE particles were significantly smaller after template removal. The size of the injectable particles is a crucial parameter; although smaller sizes below 150-nm reduce the propensity to phagocytosis, bigger particles over 500-nm have been reported to present a better hemodynamic behavior to target the wall in medium to large vessels, relevant to most cardiovascular diseases.[39, 40, 41] The size of the PASKE particles that we were able to synthesize are well adapted for application in vascular disease diagnosis and therapy. The zeta potential of the PASKE particles was slightly negative (Table S1, -9.3±3.7 mV), similar to PEG-based particles (-8.5±3.2 mV), which should favor low recognition by MPS cells.[42] We analyzed the PASK protein and the PASKE particles by liquid chromatography coupled to mass spectrometry (Figure S1) and confirmed that the protein isolated showed a mass profile matching with the PASK protein sequence (matching score 1.87×10^4) and that the PASKE particles were mainly composed of PASK protein (matching score 1.22×10^4). We studied the degradability of the particles by incubation with lysosomal cell fractions isolated from mouse tissues and confirmed their degradability within 24 h (Figure S2).

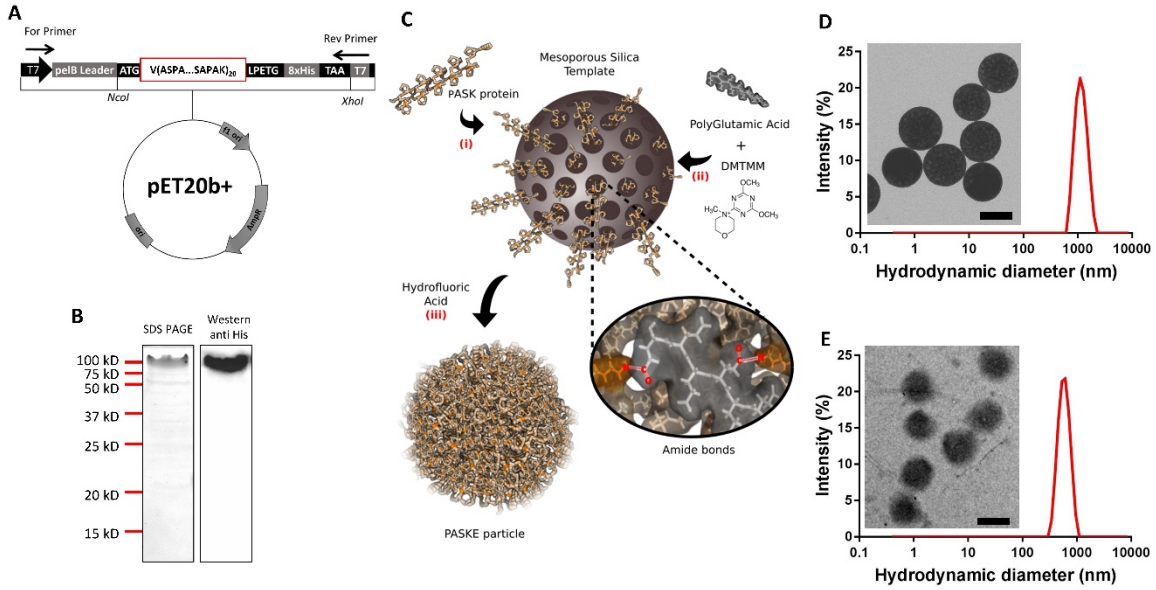

Figure 1. (**A**) Vector map of the PASK protein optimized for bacterial expression (Full sequence: MV(ASPAAPAPASPAAPAPSAPAK)$_{20}$LPETGGLE-His$_8$). (**B**) 12 % SDS-PAGE and Western blot analysis using a horseradish peroxidase coupled to anti-6XHis-tag antibody of the purified PASK protein. (**C**) Scheme of PASKE particle assembly; (i) PASKE protein is loaded into mesoporous silica template (MS) *via* electrostatic interaction, (ii) crosslinked *via* the primary amines of the lysine residues to the carboxylic groups of PolyGlutamic Acid (PGA) activated with 4-(4,6-Dimethoxy-1,3,5-triazin-2-yl)-4-methylmorpholinium chloride (DMTMM) and (iii) the MS template is dissolved 2 M Hydrofluoric acid (HF) / 8 M ammonium fluoride (NH_4F). Transmission electronic microscopy (TEM) images and size distributions obtained by dynamic light scattering (DLS) of MS@PASKE (**D**) and PASKE (**E**).

***In vitro* cell association behavior of the PASKE particles.** The low fouling properties of the PASKE particles were tested *in vitro* by incubation with murine macrophages (RAW 264.7) and human monocytic cells (THP-1), two cell lines commonly studied in phagocytosis assays (Figure

2). We compared PEG-based particles developed previously,[35, 43] bovine serum albumin (BSA) based particles to evaluate the role of the PASK protein over a commonly used model protein, and MS@PASKE particles (PASKE particles before the removal of the silica templates). As expected, the PEG particles show very low uptake and the silica particles are rapidly phagocytosed by the RAW cells (Figure 2A). The PASKE particles show a similar association profile to the PEG particles while the BSA particles associated as strongly as the MS@PASKE particles, which indicates that particles generated from PASK protein have low fouling features, unlike particles generated from *e.g.* BSA. At 24 h, PASKE particles show a slightly increased association signal (8.3±4.5 %), however non-significantly different from the PEG particles (2.3±0.5 %, p=0.67, n=5). As shown by confocal microscopy, some of the PASKE particles that show cell association at 24 h were not phagocytosed but rather stuck to the cell membrane (Figure 2C, yellow arrows) while those which were taken up seem to be degraded in the lysosomes, as shown by the diffused fluorescent signal obtained (red arrow). When using human monocytic cell line THP-1 as the target cells, we studied the effect of the addition of human plasma in the cell media to evaluate the influence of protein corona formation (Figure 2D). While the association of PEG particles remained low after the addition of plasma, the PASKE particles exhibited a delayed association behavior; the difference was small after 1 h incubation (2.4±1.7% without plasma and 5.8±2.9% with plasma, p=0.98) but markedly increased over 24 h (7.0±2.1% without plasma and 25.7±2.2% at 24 h, ***p<0.001). Imaging flow cytometry analysis of the THP-1 cells incubated for 24 h in the presence of human plasma revealed that the phagocytosed PASKE particles were preferentially localized in the lysosomes and showed signs of degradation, as indicated by the diffused fluorescence signal observed compared to the MS@PASKE particles which did not degrade (Figure 2E and F).

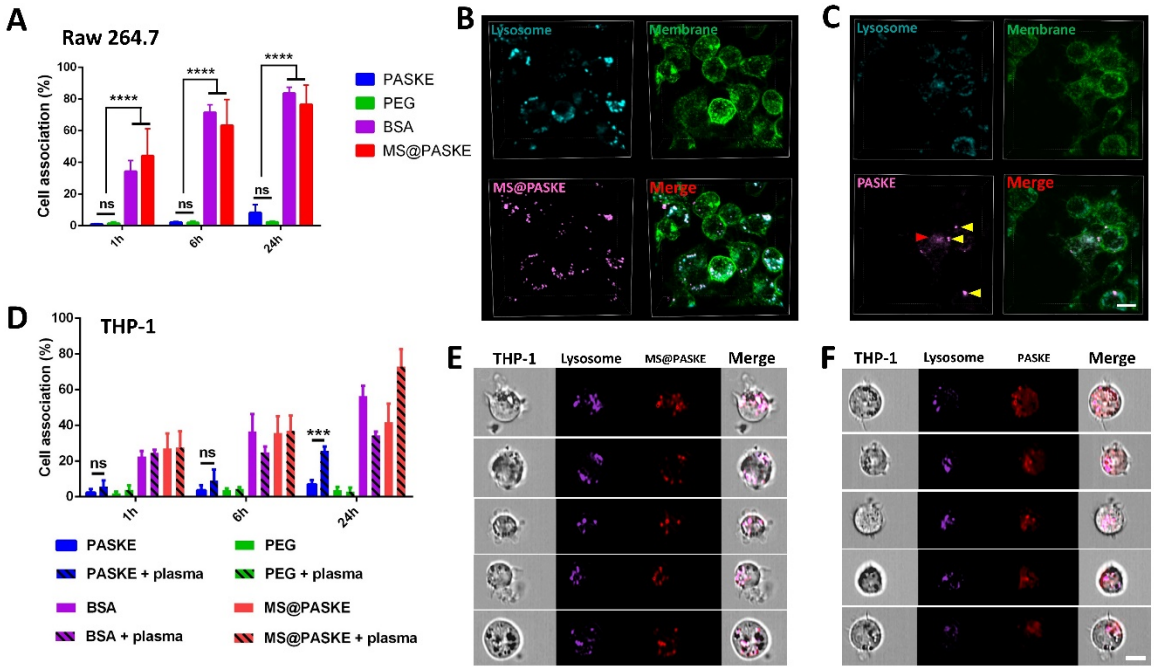

Figure 2: Cell association of PASKE, PEG, BSA and MS@PASKE with murine macrophages (RAW 264.7) and human monocytic cells (THP-1). (**A**) Cell association with RAW 264.7 cells after 1, 6 and 24 h incubation at 37 °C in Dulbecco's modified Eagle medium (DMEM) with 10% fetal calf serum (FCS) as analyzed by flow cytometry. Confocal microscopy observation of RAW 264.7 cells incubated 24 h with MS@PASKE (**B**) or PASKE (**C**) at 37 °C in DMEM medium. Particles are labelled with Cyanine 5 N-Hydroxysuccinimide (NHS) ester (Cy5, Pink), cell membrane and lysosomes were stained with Alexa Fluor 488-conjugated wheat germ agglutinin (WGA-488, green) and LysoTracker Blue DND-22 (cyan), respectively. The red arrow indicates degraded PASKE located in a lysosome, yellow arrows indicate non-degraded stuck on the surface of the cells. (**D**) Cell association with THP-1 cells as analyzed by flow cytometry after 1h, 6h and 24h at 37 °C in Roswell Park Memorial Institute (RPMI) medium with or without 10% FCS supplemented, with 200 µL of human plasma in 500 µL total volume. Representative images acquired by imaging flow cytometry of THP-1 cells incubated in RPMI supplemented with human

plasma 24 h at 37 °C with MS@PASKE (**E**) or PASKE (**F**), gated on cells positive to particle uptake. Cells are seen in bright field channel (THP-1), lysosomes are stained with LysoTracker Blue DND-22 (purple) and particles are labelled with Cy5 (red). Data are presented as the mean ± standard deviation (n=5, two-way ANOVA, ****p<0.0001, ***p<0.001, ns: non-significant). Scale bars are 10 µm.

***In vivo* fate of the PASKE particles.** The association characteristics measured in the presence of plasma were reflected *in vivo* (Figure 3). Both the MS@PASKE and BSA particles were cleared from the circulation extremely fast, with less than 10% of the injected doses present in the blood 2.5 min post-injection (Figure 3A). The PASKE particles exhibited prolonged blood clearance times as 24±7% of the particles were present after 5 min post-injection (*p<0.05). Yet, they did not circulate as long as the PEG particles, which were still present at over 38±16% in the blood after 10 min (**p<0.01). Cytometry analysis at 3 h post-injection and histology examination at 24 h post-injection of the spleen and the liver indicated that the particles were mainly sequestered in spleen macrophages and in Kupffer cells, and confirmed full degradation of the PASKE particles at 24 h (Figure 3G, yellow arrows). The tissue biodistribution study indicated that the particles preferentially accumulated in the reticuloendothelial system (Figure 3B, C and D). In accordance with the blood clearance, this accumulation occurred rapidly for the MS@PASKE particles (<30 min), relatively slowly for the PASKE particles (>30 min) and even more slowly for the PEG particles. In the PASKE group, the near infrared signal decreased significantly at 24 h in the spleen and the liver, suggesting clearance of the particles.

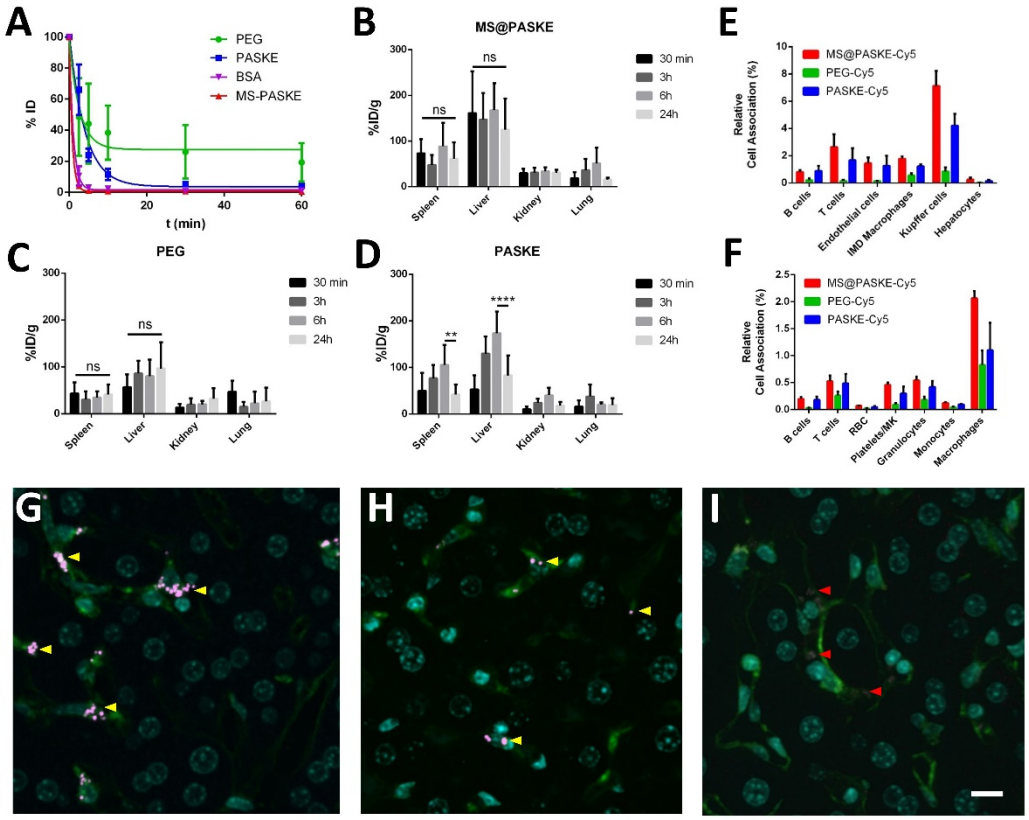

Figure 3: (**A**) Blood clearance study with PEG, PASKE, BSA and MS@PASKE. Particles were injected intravenously and counted by flow cytometry in blood samples harvested at 2.5, 5, 10, 30 and 60 minutes after injection. Mean percentage ± standard deviation from injected dose was plotted against time post-injection and exponential fit are shown (n=4, *p<0.05, ***p<0.001). Tissue biodistribution of PASKE-Cy7 (**B**), PEG-Cy7 (**C**) and MS@PASKE-Cy7 (**D**) at 30 min, 3h, 6h and 24h after intravenous injection measured with Odyssey Infrared Imaging System (n=4, two-way ANOVA, ****p<0.0001, **p<0.01, ns: non-significant). Representative scans showing the near-infrared fluorescence measured in the tissues are shown in Figure S4. Relative cell association of MS-PASKE, PEG or PASKE particles measured 3 hours after intravenous injection in different cell population of the harvested spleen (**E**) and liver (**F**). Gating strategies to identify cell type are presented in Figure S5 and S6. Data are presented as mean values ± standard deviation (n=3, *p<0.05, ***p<0.001). Histology observation of liver harvested 24 h after injection of

MS@PASKE (**G**), PEG (**H**) and PASKE (**I**). Histology observation of liver and spleen harvested 30 min Vs 24 h after injection are shown in Figure S7. Cell membrane and nuclei are stained with Alexa Fluor 488-conjugated wheat germ agglutinin (WGA-488, green) and Hoechst 33342 (cyan), respectively. Particles are labelled with Cyannine5 NHS ester (Cy5, Pink). Yellow arrows indicate non-degraded particles and red arrows indicate degraded particles. Scale bar is 20 μm.

The *in vitro* and *in vivo* data indicates that the hydrophilic conformation conferred by the Proline, Alanine and Serine repeats provide the PASKE particles with low fouling characteristics. They were not recognized immediately by immune cells and only slowly taken up by cells of the MPS in the presence of plasma. This improved the circulation time compared to albumin-based particles but the clearance still occurred faster than with the PEG particles, the low fouling gold standard. Our PASKE particles are well suited for molecular imaging of vascular diseases as the very long circulation half-life of PEG particles will result in a high blood pool background signal detrimental for an optimal signal to noise ratio.[44] The PASKE particles present an ideal compromise in blood clearance kinetics; not too fast as often encountered with most particles close to the micrometer size (*e.g.* the albumin and silica particles in this study which are eliminated within 2.5 min) but also not too slow to enable molecular imaging within a practical timeframe for medical imaging. At 20 minutes post-injection the PASKE particles would not show background signal whereas the PEG particles were still present at around 25% of the injected dose. In addition, this optimized clearance time is required for the cells from the MPS to clear the injected materials from the body thereby avoiding unspecific accumulation and potential long-term toxicity. The recent Food and Drug Administration draft guidelines for the assessment of nanomaterials toxicity specifically addresses the concerns regarding the risk related to the chronic exposure to accumulated non-

biodegradable components.[45] The PASKE particles are excellent candidates in that context, as they demonstrate full biodegradability within 24 hours.

Molecular imaging of thrombosis. Based on these favorable results, we examined the suitability of the PASKE particle platform for imaging applications and developed a molecular imaging tool to visualize activated platelets in the setting of thrombosis. We functionalized the PASKE particles with the previously described single-chain antibody specific to the activated form of the Glycoprotein IIb/IIIa (GPIIb/IIIa, anti-GPIIb/IIIa-scFv),[46] the most prominent marker expressed by platelets upon activation (Figure 4). For that purpose, we first modified the anti-GPIIb/IIIa-scFv *via* the Sortase A enzymatic conjugation technique with a bicyclo[6.1.0]nonyne (BCN) group, then we coated the PASKE particles with azide group (N_3) and finally we attached the BCN modified anti-GPIIb/IIIa-scFv at the surface of the PASKE-N_3 by copper-free click chemistry (Figure S3). The affinity of the PASKE-anti-GPIIb/IIIa-scFv for thrombosis was tested *in vitro* in microfluidic channels on micro thrombi formed from human blood (Figure 4 A, B, C and video S1, S2) and *in vivo* on a mouse model of thrombosis in mesenteric vessels (Figure 4 D, E, F). Both experiments demonstrate substantial targeting to the microthrombi compared to PASKE particles functionalized with the Mut-scFv non-binding control scFv. The efficient targeting observed in our study is supported by the margination effect from which particles with this size range benefit.[40, 41, 47] However, in a flow chamber system mimicking vascular wall targeting, others have shown that larger particles experience stronger shear detachment forces and that 200 nm particles exhibit improved binding compared to 1-2 μm particles.[48] The PASKE-anti-GPIIb/IIIa-scFv were then labelled with Cyanine 7 NHS ester and we tested their capacity to detect carotid thrombosis in mice with a Spectrum *In Vivo* Imaging System (IVIS) in near-infrared fluorescence. The PASKE-

anti-GPIIb/IIIa-scFv-Cy7 resulted in a significant signal uptake of the carotid thrombosis over the non-targeted (PASKE-Mut-scFv-Cy7) and vehicle control (Figure 4 G, H). The accumulation of the targeted PASKE particles in the thrombotic carotid artery was confirmed by imaging the particles using a near infrared (NIR) confocal microscope setup we implemented (Figure 4 I, J).

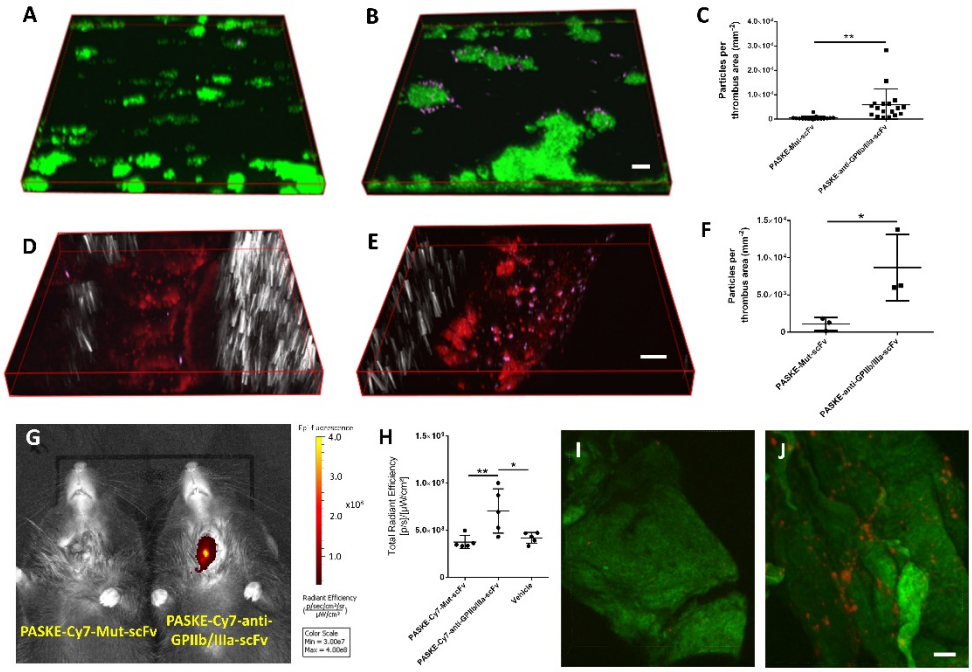

Figure 4: PASKE particles functionalized with the anti-GPIIb/IIIa scFv (following the procedure presented in figure S3) to convey specific affinity to activated platelets.

The targeting properties were tested *in vitro* in flow condition over microthrombi formed from human blood in microfluidic channels. The platelets were stained with 3,30-dihexyloxacarbocyanine iodide ($DiOC_6$, 0.5 µg mL^{-1}) and are seen in the 488-nm channel shown in green. Cy5 labelled particles, seen in the 640-nm channel, are flown over the top of the platelet-rich microthrombi at a shear rate fixed at 300 s^{-1} for 3 minutes. Representative Z-stack acquisitions after flowing PASKE-Cy5-Mut-scFv (**A**) and PASKE-Cy5-anti-GPIIb/IIIa (**B**) are shown. Time-

lapse Z-stack acquisitions are provided as video files in the Supporting information. (**C**) Mean values of particles per mm^2 of thrombi ± SD (n=17, **p<0.01, non-parametric t-test). PASKE-Cy5-Mut-scFv (**D**) and PASKE-Cy5-anti-GPIIb/IIIa (**E**) interaction on thrombotic micro vessels from mice mesentery observed by confocal microscopy. Platelets and leukocytes were labelled with Rhodamine 6G (0.3% w/v) and observed in the 561-nm channel and Cy5 particles in the 640-nm channel. (**F**) Mean values of particles per mm^2 of thrombi ± SD (n=3, *p<0.05, non-parametric t-test). (**G**) Carotid thrombosis near infrared fluorescence imaging with a spectrum *in vivo* imaging system (IVIS) after injection of PASKE-Cy7-Mut-scFv (left) or PASKE-Cy7-anti-GPIIb/IIIa (right). (**H**) Signal quantification over the left carotid area expressed as total radiant efficiency ± SD (photons per second per micro watt squared centimeter, $p.s^{-1}.\mu W^{-1}.cm^2$, n=3). Confocal microscopy observation of the thrombotic carotid artery after injection of PASKE-Cy7-Mut-scFv (**I**) or PASKE-Cy7-anti-GPIIb/IIIa (**J**). Vessel wall was seen in auto-fluorescence in 488-nm channel and Cy7 labelled particles were detected with a near-infrared laser in the 780-nm channel. Scale bars are 20 μm for A and B and 100 μm for D, E, I and J.

Transmigration ability of the PASKE particles on inflamed endothelium. Another potentially interesting application for our particle platform is the development of injectable carriers that cross biological barriers and reach locations non-accessible by soluble molecule.[49, 50, 51] We tested the capacity of the PASKE particles to cross an inflamed confluent monolayer of human primary Human umbilical vein endothelial cells (HUVEC) and observed a significant amount of crossing particles when tumor necrosis factor alpha (TNFα) was added to induce inflammation (Figure 5). This indicates that the PASKE particles have high potential to deliver anti-inflammatory drugs

through activated endothelium and reduce the pathological inflammation within the media layer, a relevant situation in several vascular diseases such as atherosclerosis or aneurysms.

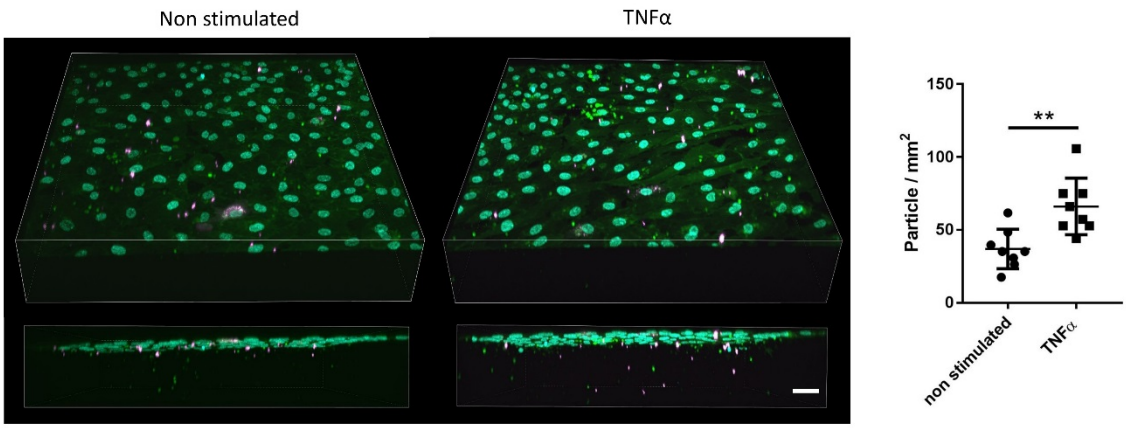

Figure 5: *In vitro* transmigration of PASKE particles across HUVEC monolayers. HUVECs were cultivated to form a confluent monolayer on a collagen matrix. PASKE-Cy5 particles were added on top of non-activated HUVEC *versus* HUVEC stimulated with TNFα. Confocal microscopy enabled observation in the 640-nm channel to identify transmigration of PASKE-Cy5 particles. The number of particles that crossed the cell monolayer was quantified and presented as the mean number of particles per mm^2 ± SD (n=8, **p<0.01). Scale bar is 100 µm.

CONCLUSIONS

We have synthesized protein-based particles from hydrophilic proline-alanine-serine rich protein blocks crosslinked with poly(L-glutamic acid) using mesoporous silica templating. The so-called PASKE particles present specific low fouling features that provide blood clearance kinetics well suited for molecular imaging and were found to be biodegradable within 24 h in the lysosomes of cells from the mononuclear phagocytic system. Moreover, this versatile injectable platform was successfully functionalized with an activated platelet specific scFv *via* Sortase conjugation and click chemistry and labelled with a near-infrared fluorescent molecule. We demonstrated the

potential application of the PASKE particle as a platelet-rich thrombus molecular imaging tool in a carotid thrombosis mouse model and we showed their capacity to cross the inflamed endothelium *in vitro*.

METHODS SECTION

Production of PASK protein and synthesis of PASKE particles: PASK protein building blocks (full amino acid sequence: MV(ASPAAPAPASPAAPAPSAPAK)$_{20}$LPETGGLE-His$_8$) were produced recombinantly (full description provided in the Supporting Information) and assembled into PASKE particles *via* the MS templating technique. MS templates of ~1200-nm diameter were prepared following a previously published method.[52] Poly(ethylene glycol) (PEG) particles were synthesized following a previously described protocol.[35]

Particle characterization: Full details of transmission electron microscopy (TEM) observation, zeta potential measurement, diffracted light scattering size analysis, mass spectroscopy, cell association assays, biodegradability tests, functionalization of PASKE with anti-GPIIb/IIIa and Mut-scFv scFvs, flow chamber experiment and cell migration experiment are provided in the Supporting Information.

Animal experiments: All experiments involving animals were approved by the Alfred Medical Research and Education Precinct Animal Ethics Committee (E/1625/2016/M, E/1534/2015/B and E/1589/2015/B). 6 weeks old C57Bl6 mice were anaesthetized and $10^6.g^{-1}$ of PASKE, PEG, BSA and MS@PASKE particles were injected intravenously. For biodistribution study and thrombosis imaging, Cy7 labelled particles were used. Mice were culled and perfused at 30 min, 3 h, 6 h and 24 h after injection, tissues of interest (the spleen, a part of the liver, the left kidney and the lung) were harvested, weighed and scanned using Odyssey CLx Infrared Imaging System (LI-COR,

Biosciences). Fluorescence signal was measured in the 800-nm channel, in the tissues and in the injected suspensions, and tissue biodistribution values were expressed as mean values of percentage of injected dose per gram of tissue ± SD (% ID.g^{-1}, n=4). Blood clearance, liver/spleen cell distribution and histology methods are fully described in the Supporting Information. Mesenteric and carotid thrombosis models were performed as described elsewhere.[53] Briefly, mice were anaesthetized, mesentery were gently exteriorized through a midline abdominal incision, platelet and leukocytes were labelled with intravenous injection of Rhodamine 6G (30 µL, 0.3 % w/v, in PBS, Sigma Aldrich), thrombosis was induced by deposition of a small piece of filter paper soaked with ferric chloride ($FeCl_3$, 20% w/v in PBS, Sigma Aldrich) on the vessel of interest. Thrombosis formation was observed by intravital confocal microscopy (A1R+, Nikon) monitoring platelet aggregation in the 561-nm channel. After 2 minutes of $FeCl_3$ exposure, the vessel was rinsed with warm PBS and PASKE-Cy5-anti-GPIIb/IIIa-scFv or PASKE-Cy5-Mut-scFv were injected. Time-lapse Z-stack acquisitions were performed within the first 5 minutes post-injection and then a range of images were taken along the thrombotic vessels. From one representative image per mouse, the amount of thrombus was measured in the 561-nm channel images with Image J (NIH, USA) and expressed as the area of surface coverage (in mm^2). The PASKE-Cy5-anti-GPIIb/IIIa-scFv or PASKE-Cy5-Mut-scFv adherent to the micro thrombi were counted in the 640-nm channel images. Results are presented as mean values of particles per mm^2 of thrombi ± SD (n=3).

For the carotid artery thrombosis model, a small incision below the jaw down to the sternum was performed and a 5-mm fragment of the left external carotid was isolated, thrombosis was induced by deposition of a small piece of filter paper soaked with ferric chloride (20% w/v in PBS, Sigma Aldrich) on the artery. After 3 min of ferric chloride exposure, the PASKE-Cy7-anti-GPIIb/IIIa-

scFv, the PASKE-Cy7-Mut-scFv or the vehicle control (PBS) were injected intravenously then the filter paper is removed, the carotid artery area is washed with PBS and dried. Mice were then scanned 20 minutes after injection with a spectrum *in vivo* imaging system (Caliper IVIS Lumina II Imaging System, PerkinElmer) at 720- and 790-nm excitation and emission filters, respectively. Imaging parameters were set as follows: medium binning, apertur size FStop=2, subject height = 1.50 cm and field of view = 12.5 cm^2 or 6.5 cm^2. The signal was quantified over the left carotid area and expressed as total radiant efficiency ± SD (photons per second per micro watt squared centimeter, $p.s^{-1}.\mu W^{-1}.cm^2$, n=3). Carotid arteries were then harvested, washed in PBS, fixed in formalin and observed by confocal microscopy (A1R+, Nikon); vessel wall was seen in auto fluorescence in 488-nm channel and Cy7 labelled particles were detected with a near-infrared confocal microscope in the 780-nm channel.

ACKNOWLEDGMENTS

This work was funded by the National Health and Medical Research Council (NHMRC, Project Grant 1078118 to C.E.H.) and the National Heart Foundation of Australia (Fellowship CR11M6066 to C.E.H.). F.C. acknowledges the award of an NHMRC Senior Principal Research Fellowship (APP1135806). This research was also funded by the Australian Research Council (ARC) Centre of Excellence in Convergent Bio-Nano Science and Technology (Project Number CE140100036) and funded by the ARC under the Australian Laureate Fellowship (FL120100030) scheme. T.B. has received funding from the People Programme (Marie Curie Actions) of the European Union's Seventh Framework Programme (FP7/2007-2013) under REA grant agreement nº 608765. J.C. acknowledges the Thousand Talent Plan Program of China.

We thank Dr D. Steer from the Monash Biochemical Proteomics Facility, C. Cohen and A. Shad from the Monash Histology Platform, E. Orlowski-Oliver from the AMREP flow core, Dr I. Carmichael from Monash Micro Imaging, and J. Tran for technical advice and assistance. We thank Prof P.S. Donnelly and Dr T.U. Connell for providing the G-PEG_3-BCN compound.

Supporting Information Available:

Supporting methods section and figures (PDF).

Video files showing the targeting capacities of the PASKE particles to microthrombi in a microfluidic system. Video 1 (avi) shows the non-binding control with the PASKE-Mut-scFv and Video 2 (avi) shows the PASKE-anti-GPII/IIIa-scFv exhibiting strong affinity for the microthrombi.

This material is available free of charge *via* the Internet at http://pubs.acs.org.

REFERENCES

1. Etheridge, M. L.; Campbell, S. A.; Erdman, A. G.; Haynes, C. L.; Wolf, S. M.; McCullough, J., The Big Picture on Nanomedicine: The State of Investigational and Approved Nanomedicine Products. *Nanomedicine* **2013,** *9*, 1-14.

2. Mitragotri, S.; Anderson, D. G.; Chen, X.; Chow, E. K.; Ho, D.; Kabanov, A. V.; Karp, J. M.; Kataoka, K.; Mirkin, C. A.; Petrosko, S. H.; Shi, J.; Stevens, M. M.; Sun, S.; Teoh, S.; Venkatraman, S. S.; Xia, Y.; Wang, S.; Gu, Z.; Xu, C., Accelerating the Translation of Nanomaterials in Biomedicine. *ACS Nano* **2015,** *9*, 6644-6654.

3. Radomska, A.; Leszczyszyn, J.; Radomski, M. W., The Nanopharmacology and Nanotoxicology of Nanomaterials: New Opportunities and Challenges. *Adv Clin Exp Med* **2016,** *25*, 151-162.

4. Seo, S.-J.; Chen, M.; Wang, H.; Min Sil, K.; Leong, K.; Kim, H.-W., Extra- and Intra-Cellular Fate of Nanocarriers under Dynamic Interactions with Biology. *Nano Today* **2017**, *14*, 84-99.

5. Polo, E.; Collado, M.; Pelaz, B.; del Pino, P., Advances toward More Efficient Targeted Delivery of Nanoparticles *in Vivo*: Understanding Interactions between Nanoparticles and Cells. *ACS Nano* **2017,** *11*, 2397-2402.

6. Gustafson, H. H.; Holt-Casper, D.; Grainger, D. W.; Ghandehari, H., Nanoparticle Uptake: The Phagocyte Problem. *Nano today* **2015,** *10*, 487-510.

7. Behzadi, S.; Serpooshan, V.; Tao, W.; Hamaly, M. A.; Alkawareek, M. Y.; Dreaden, E. C.; Brown, D.; Alkilany, A. M.; Farokhzad, O. C.; Mahmoudi, M., Cellular Uptake of Nanoparticles: Journey Inside the Cell. *Chem Soc Rev* **2017,** *46*, 4218-4244.

8. Lowe, S.; O'Brien-Simpson, N. M.; Connal, L. A., Antibiofouling Polymer Interfaces: Poly(Ethylene Glycol) and Other Promising Candidates. *Polym Chem* **2015,** *6*, 198-212.

9. Klibanov, A. L.; Maruyama, K.; Torchilin, V. P.; Huang, L., Amphipathic Polyethyleneglycols Effectively Prolong the Circulation Time of Liposomes. *FEBS Lett* **1990,** *268*, 235-237.

10. Karakoti, A. S.; Das, S.; Thevuthasan, S.; Seal, S., PEGylated Inorganic Nanoparticles. *Angew Chem Int Ed Engl* **2011,** *50*, 1980-1994.

11. Jokerst, J. V.; Lobovkina, T.; Zare, R. N.; Gambhir, S. S., Nanoparticle PEGylation for Imaging and Therapy. *Nanomedicine (Lond)* **2011,** *6*, 715-728.

12. Amoozgar, Z.; Yeo, Y., Recent Advances in Stealth Coating of Nanoparticle Drug Delivery Systems. *Wiley Interdiscip Rev Nanomed Nanobiotechnol* **2012,** *4*, 219-233.

13. Weissig, V.; Pettinger, T. K.; Murdock, N., Nanopharmaceuticals (Part 1): Products on the Market. *Int J Nanomedicine* **2014,** *9*, 4357-4373.

14. Knop, K.; Hoogenboom, R.; Fischer, D.; Schubert, U. S., Poly(Ethylene Glycol) in Drug Delivery: Pros and Cons As Well As Potential Alternatives. *Angew Chem Int Ed Engl* **2010,** *49*, 6288-6308.

15. Romberg, B.; Metselaar, J. M.; Baranyi, L.; Snel, C. J.; Bunger, R.; Hennink, W. E.; Szebeni, J.; Storm, G., Poly(Amino Acid)s: Promising Enzymatically Degradable Stealth Coatings for Liposomes. *Int J Pharm* **2007,** *331*, 186-189.

16. Rudmann, D. G.; Alston, J. T.; Hanson, J. C.; Heidel, S., High Molecular Weight Polyethylene Glycol Cellular Distribution and PEG-associated Cytoplasmic Vacuolation is Molecular Weight Dependent and Does Not Require Conjugation to Proteins. *Toxicol Pathol* **2013,** *41*, 970-983.

17. Abu Lila, A. S.; Kiwada, H.; Ishida, T., The Accelerated Blood Clearance (ABC) Phenomenon: Clinical Challenge and Approaches to Manage. *J Control Release* **2013,** *172*, 38-47.

18. Dams, E. T.; Laverman, P.; Oyen, W. J.; Storm, G.; Scherphof, G. L.; van der Meer, J. W.; Corstens, F. H.; Boerman, O. C., Accelerated Blood Clearance and Altered Biodistribution of Repeated Injections of Sterically Stabilized Liposomes. *J Pharmacol Exp Ther* **2000,** *292*, 1071-1079.

19. Banerjee, I.; Pangule, R. C.; Kane, R. S., Antifouling Coatings: Recent Developments in the Design of Surfaces That Prevent Fouling by Proteins, Bacteria, and Marine Organisms. *Adv Mater* **2011,** *23*, 690-718.

20. Schlapschy, M.; Theobald, I.; Mack, H.; Schottelius, M.; Wester, H. J.; Skerra, A., Fusion of a Recombinant Antibody Fragment with a Homo-Amino-Acid Polymer: Effects on Biophysical Properties and Prolonged Plasma Half-life. *Protein Eng Des Sel* **2007,** *20*, 273-284.

21. Schlapschy, M.; Binder, U.; Borger, C.; Theobald, I.; Wachinger, K.; Kisling, S.; Haller, D.; Skerra, A., PASylation: A Biological Alternative to PEGylation for Extending the Plasma Half-Life of Pharmaceutically Active Proteins. *Protein Eng Des Sel* **2013,** *26*, 489-501.

22. Mendler, C. T.; Friedrich, L.; Laitinen, I.; Schlapschy, M.; Schwaiger, M.; Wester, H. J.; Skerra, A., High Contrast Tumor Imaging with Radio-Labeled Antibody Fab Fragments Tailored for Optimized Pharmacokinetics *Via* PASylation. *MAbs* **2015,** *7*, 96-109.

23. Falvo, E.; Tremante, E.; Arcovito, A.; Papi, M.; Elad, N.; Boffi, A.; Morea, V.; Conti, G.; Toffoli, G.; Fracasso, G.; Giacomini, P.; Ceci, P., Improved Doxorubicin Encapsulation and Pharmacokinetics of Ferritin-Fusion Protein Nanocarriers Bearing Proline, Serine, and Alanine Elements. *Biomacromolecules* **2016,** *17*, 514-522.

24. Kuhn, N.; Schmidt, C. Q.; Schlapschy, M.; Skerra, A., PASylated Coversin, a C5-Specific Complement Inhibitor with Extended Pharmacokinetics, Shows Enhanced Anti-Hemolytic Activity *in Vitro*. *Bioconjug Chem* **2016,** *27*, 2359-2371.

25. Croissant, J. G.; Fatieiev, Y.; Khashab, N. M., Degradability and Clearance of Silicon, Organosilica, Silsesquioxane, Silica Mixed Oxide, and Mesoporous Silica Nanoparticles. *Adv Mater* **2017,** *29*.

26. Longmire, M.; Choyke, P. L.; Kobayashi, H., Clearance Properties of Nano-Sized Particles and Molecules as Imaging Agents: Considerations and Caveats. *Nanomedicine (Lond)* **2008,** *3*, 703-717.

27. Duro-Castano, A.; Nebot, V. J.; Nino-Pariente, A.; Arminan, A.; Arroyo-Crespo, J. J.; Paul, A.; Feiner-Gracia, N.; Albertazzi, L.; Vicent, M. J., Capturing "Extraordinary" Soft-Assembled Charge-Like Polypeptides As a Strategy for Nanocarrier Design. *Adv Mater* **2017,** *29*.

28. Kolosnjaj-Tabi, J.; Lartigue, L.; Javed, Y.; Luciani, N.; Pellegrino, T.; Wilhelm, C.; Alloyeau, D.; Gazeau, F., Biotransformations of Magnetic Nanoparticles in the Body. *Nano Today* **2016,** *11*, 280-284.

29. Campbell, F.; Bos, F. L.; Sieber, S.; Arias-Alpizar, G.; Koch, B. E.; Huwyler, J.; Kros, A.; Bussmann, J., Directing Nanoparticle Biodistribution through Evasion and Exploitation of Stab2-Dependent Nanoparticle Uptake. *ACS Nano* **2018,** *12*, 2138-2150.

30. Yin, B.; Li, K. H. K.; Ho, L. W. C.; Chan, C. K. W.; Choi, C. H. J., Toward Understanding *in Vivo* Sequestration of Nanoparticles at the Molecular Level. *ACS Nano* **2018,** *12*, 2088-2093.

31. Grove, T. Z.; Cortajarena, A. L. Protein Design for Nanostructural Engineering: Concluding Remarks and Future Directions. In *Protein-based Engineered Nanostructures;* Cortajarena, A. L., Grove, T. Z., Eds.; Springer: 940, **2016**; pp 281-284.

32. Brix, K., Lysosomal Proteases. *Lysosomes* **2005**, *5*, 50-59.

33. Akagi, T.; Higashi, M.; Kaneko, T.; Kida, T.; Akashi, M., Hydrolytic and Enzymatic Degradation of Nanoparticles Based on Amphiphilic Poly(Gamma-Glutamic Acid)-Graft-L-Phenylalanine Copolymers. *Biomacromolecules* **2006,** *7*, 297-303.

34. Bajaj, I.; Singhal, R., Poly (Glutamic Acid)--An Emerging Biopolymer of Commercial Interest. *Bioresour Technol* **2011,** *102*, 5551-5561.

35. Cui, J.; De Rose, R.; Alt, K.; Alcantara, S.; Paterson, B. M.; Liang, K.; Hu, M.; Richardson, J. J.; Yan, Y.; Jeffery, C. M.; Price, R. I.; Peter, K.; Hagemeyer, C. E.; Donnelly, P. S.; Kent, S. J.; Caruso, F., Engineering Poly(Ethylene Glycol) Particles for Improved Biodistribution. *ACS Nano* **2015,** *9*, 1571-1580.

36. Cui, J.; De Rose, R.; Best, J. P.; Johnston, A. P.; Alcantara, S.; Liang, K.; Such, G. K.; Kent, S. J.; Caruso, F., Mechanically Tunable, Self-Adjuvanting Nanoengineered Polypeptide Particles. *Adv Mater* **2013,** *25*, 3468-3472.

37. Cui, J.; Yan, Y.; Wang, Y.; Caruso, F., Templated Assembly of pH-Labile Polymer-Drug Particles for Intracellular Drug Delivery. *Adv Funct Mater* **2012,** *22*, 4718-4723.

38. Suma, T.; Cui, J.; Mullner, M.; Fu, S.; Tran, J.; Noi, K. F.; Ju, Y.; Caruso, F., Modulated Fragmentation of Proapoptotic Peptide Nanoparticles Regulates Cytotoxicity. *J Am Chem Soc* **2017,** *139*, 4009-4018.

39. Zhang, S.; Gao, H.; Bao, G., Physical Principles of Nanoparticle Cellular Endocytosis. *ACS Nano* **2015,** *9*, 8655-8671.

40. Namdee, K.; Thompson, A. J.; Charoenphol, P.; Eniola-Adefeso, O., Margination Propensity of Vascular-Targeted Spheres from Blood Flow in a Microfluidic Model of Human Microvessels. *Langmuir* **2013,** *29*, 2530-2535.

41. Muller, K.; Fedosov, D. A.; Gompper, G., Margination of Micro- and Nano-Particles in Blood Flow and Its Effect on Drug Delivery. *Sci Rep* **2014,** *4*, 4871.

42. He, C.; Hu, Y.; Yin, L.; Tang, C.; Yin, C., Effects of Particle Size and Surface Charge on Cellular Uptake and Biodistribution of Polymeric Nanoparticles. *Biomaterials* **2010,** *31*, 3657-3666.

43. Cui, J.; Bjornmalm, M.; Liang, K.; Xu, C.; Best, J. P.; Zhang, X.; Caruso, F., Super-Soft Hydrogel Particles with Tunable Elasticity in a Microfluidic Blood Capillary Model. *Adv Mater* **2014,** *26*, 7295-7299.

44. Lohrke, J.; Siebeneicher, H.; Berger, M.; Reinhardt, M.; Berndt, M.; Mueller, A.; Zerna, M.; Koglin, N.; Oden, F.; Bauser, M.; Friebe, M.; Dinkelborg, L. M.; Huetter, J.; Stephens, A. W., (18)F-GP1, a Novel PET Tracer Designed for High-Sensitivity, Low-Background Detection of Thrombi. *J Nucl Med* **2017,** *58*, 1094-1099.

45. U.S. Food and Drug Administration, Drug Products, Including Biological Products, That Contain Nanomaterials; Draft Guidance for Industry Federal Register **2017**, *82*, 241.

46. Bonnard, T.; Tennant, Z.; Niego, B.; Kanojia, R.; Alt, K.; Jagdale, S.; Law, L. S.; Rigby, S.; Medcalf, R. L.; Peter, K.; Hagemeyer, C. E., Novel Thrombolytic Drug Based on Thrombin Cleavable Microplasminogen Coupled to a Single-Chain Antibody Specific for Activated GPIIb/IIIa. *J Am Heart Assoc* **2017,** *6*, e004535.

47. Forouzandehmehr, M.; Shamloo, A., Margination and Adhesion of Micro- and Nanoparticles in the Coronary Circulation: A Step Towards Optimised Drug Carrier Design. *Biomech Model Mechanobiol* **2018,** *17*, 205-221.

48. Anselmo, A. C.; Modery-Pawlowski, C. L.; Menegatti, S.; Kumar, S.; Vogus, D. R.; Tian, L. L.; Chen, M.; Squires, T. M.; Sen Gupta, A.; Mitragotri, S., Platelet-Like Nanoparticles: Mimicking Shape, Flexibility, and Surface Biology of Platelets to Target Vascular Injuries. *ACS Nano* **2014,** *8*, 11243-11253.

49. Blanco, E.; Shen, H.; Ferrari, M., Principles of Nanoparticle Design for Overcoming Biological Barriers to Drug Delivery. *Nat Biotechnol* **2015,** *33*, 941-951.

50. Lobatto, M. E.; Calcagno, C.; Millon, A.; Senders, M. L.; Fay, F.; Robson, P. M.; Ramachandran, S.; Binderup, T.; Paridaans, M. P.; Sensarn, S.; Rogalla, S.; Gordon, R. E.; Cardoso, L.; Storm, G.; Metselaar, J. M.; Contag, C. H.; Stroes, E. S.; Fayad, Z. A.; Mulder, W. J., Atherosclerotic Plaque Targeting Mechanism of Long-Circulating Nanoparticles Established by Multimodal Imaging. *ACS Nano* **2015,** *9*, 1837-1847.

51. Duivenvoorden, R.; Tang, J.; Cormode, D. P.; Mieszawska, A. J.; Izquierdo-Garcia, D.; Ozcan, C.; Otten, M. J.; Zaidi, N.; Lobatto, M. E.; van Rijs, S. M.; Priem, B.; Kuan, E. L.; Martel, C.; Hewing, B.; Sager, H.; Nahrendorf, M.; Randolph, G. J.; Stroes, E. S.; Fuster, V.; Fisher, E. A.; *et al.* Statin-Loaded Reconstituted High-Density Lipoprotein Nanoparticle Inhibits Atherosclerotic Plaque Inflammation. *Nat Commun* **2014,** *5*, 3065.

52. Wang, J.-G.; Zhou, H.-J.; Sun, P.-C.; Ding, D.-T.; Chen, T.-H., Hollow Carved Single-Crystal Mesoporous Silica Templated by Mesomorphous Polyelectrolyte−Surfactant Complexes. *Chem Mater* **2010,** *22*, 3829-3831.

53. Bonnard, T.; Hagemeyer, C. E., Ferric Chloride-Induced Thrombosis Mouse Model on Carotid Artery and Mesentery Vessel. *J Vis Exp* **2015**, e52838.

Low Fouling and Biodegradable Protein-Based Particles for Thrombus Imaging (supplementary information)

Thomas Bonnard[†], Anand Jayapadman[†], Jasmine A. Putri[†], Jiwei Cui[§‡], Yi Ju[§], Catherine Carmichael[#], Thomas A. Angelovich[¥], Stephen H. Cody[ꟾ], Shauna French[⌘], Karline Pascaud[†], Hannah A. Pearce[†], Shweta Jagdale[†], Frank Caruso[§], Christoph E. Hagemeyer[†]*

[†]Nanobiotechnology Laboratory, Australian Centre for Blood Diseases, Central Clinical School, Monash University, Melbourne 3004, Victoria, Australia.

[§]ARC Centre of Excellence in Convergent Bio-Nano Science and Technology, and the Department of Chemical Engineering, The University of Melbourne, Parkville, Victoria 3010, Australia.

[‡]Key Laboratory of Colloid and Interface Chemistry of the Ministry of Education, and the School of Chemistry and Chemical Engineering, Shandong University, Jinan 250100, China.

[#]Mammalian Functional Genetics Laboratory, Australian Centre for Blood Diseases, Central Clinical School, Monash University, Melbourne 3004, Victoria, Australia.

[¥]Chronic Infectious and Inflammatory Diseases Program, School of Health and Biomedical Sciences, RMIT University, Melbourne, Australia and Life Sciences, Burnet Institute, Melbourne, Australia.

[ꟾ]Monash Micro Imaging, Monash University, Melbourne 3004, Victoria, Australia.

[⌘] Platelets and Thrombosis Laboratory, Australian Centre for Blood Diseases, Central Clinical School, Monash University, Melbourne 3004, Victoria, Australia.

*Send email correspondence to christoph.hagemeyer@monash.edu

SUPPORTING METHODS SECTION

Generation, expression and purification of PASK protein building blocks. The DNA sequence encoding the PASK protein (full amino acid sequence: MV(ASPAAPAPASPAAPAPSAPAK)$_{20}$LPETGGLE-His$_8$) codon optimized for bacterial expression, and flanked by the restriction sites NcoI and XhoI, was ordered from Geneart and transformed into NEB Turbo competent cells. DNA was prepped using a Qiagen plasmid mini kit and digested with NcoI and XhoI (NEB). The resultant 1382bp fragment was run on and excised from a 0.8% agarose gel, and purified using a QIAGEN plasmid gel extraction kit. pET20b+ (Novagen) was prepared equivalently. The construct was then ligated into the multiple cloning site of pET20b+ with T4 DNA Ligase (NEB) and subsequently transformed into NEB Turbo competent cells. Colony screening PCR was used to determine successful ligation, with GoTaq Green master mix (Promega). Primers flanked the multiple cloning site and annealed to the T7 promoter and terminator sequences (Novagen). A successful ligation was indicated by a 1567bp amplicon. Plasmid preparations of positive colonies were sent to AGRF for sequencing, with the same primers as for colony screening PCR, and the Emboss Needle sequence alignment tool was used to confirm a match with the expected sequence. DNA confirmed as MV(ASPAAPAPASPAAPAPSAPAK)$_{20}$LPETGGLE-His$_8$ correctly inserted into pET20b+ was transformed into One Shot® BL21 Star™ (DE3) cells for expression in *E. coli*. The cells were cultured in LB media containing 100 μg/mL ampicillin until the OD600 of 0.8 was reached. PASK production was induced with 1 mmol L^{-1} of isopropyl β-D-1-thiogalactopyranoside (IPTG) for 4 hours at 37^{o}C. Bacteria were then isolated by centrifugation at 6000 rcf for 10 min. Proteins were purified by fast liquid protein chromatography using Ni-NTA column (Invitrogen) followed by size exclusion chromatography (Superose 12, 10/300 GL, GE Healthcare), according to the

manufacturer's protocol. Protein concentration was determined with a Direct Detect Infrared Spectrometer (Merck, Millipore). The purity of the proteins was analyzed by SDS-PAGE gel stained with Coomassie Brilliant Blue visualized using a BioRad Gel-Doc system. Western blot analysis was performed to confirm the presence of the PASK protein by revealing the 8xHis-tag. After SDS-gel electrophoresis, the proteins were transferred on polyvinylidene difluoride (PVDF) membranes which were blocked with 5% skimmed milk at 4°C overnight then incubated for 1 hour with Anti-6xHis-tag antibody HRP (horse radish peroxidase). Detection was performed with SuperSignal West Pico chemiluminescent (ECL) substrate (Thermo Scientific) for the HRP enzyme. The ECL signal on membranes was visualized using a BioRad Gel-Doc system.

Assembly of PASKE particles. Mesoporous silica (MS) particles (3 mg) were washed with phosphate buffer (PB, 10 mM, pH 7.4) and incubated in 300 µL of PASK building blocks solution at 5 mg mL^{-1} in PB under constant shaking overnight. The MS@PASK particles were then isolated by centrifugation and washed three times with PB, followed by labeling with 5 µL of Cyanine 7 or Cyanine 5 succinimidyl ester (NHS-Cy7 or NHS-Cy5, Lumiprobe, 1 mg mL^{-1}) in 100 µL PB for 10 min. 100 µL Poly-L-glutamic acid (PGA, 1.5 kDa, 1.5 mg, Sigma Aldrich, US) was mixed with 100 µL of 4-(4,6-Dimethoxy-1,3,5-triazin-2-yl)-4-methylmorpholinium chloride (DMTMM, 4.5 mg) (Sigma Aldrich, Australia) and incubated for 15 minutes at room temperature while mixing. Crosslinking of PASK protein within the templates between the primary amines of lysine residues and activated carboxylate groups of glutamic acid residues was done by adding 200 µL of PGA and DMTMM mixture to PASK-loaded MS particle suspension and incubated overnight at room temperature. After three washing cycles with water, the MS@PASKE were resuspended in PB (10 mM). For the preparation of the PASKE particles, MS templates were removed with a 2 M Hydrofluoric acid/8 M Ammonium fluoride solution. Bovine serum albumin (BSA) based

particles were synthesized following similar method replacing PASK protein by BSA (Sigma Aldrich).

Mass spectrometry analysis. The samples were reduced and alkylated with DTT\Iodoacetamide and digested overnight with trypsin in a total of 50 uL of 20 mM ammonium bicarbonate buffer. Tryptic digests were analyzed by liquid chromatography coupled to mass spectrometry (LC-MS/MS) (LC: Ultimate 3000 nano RSLC, MS: QExactive mass spectrometer, ThermoFisher Scientific) by separation over a 30-minute gradient on a Thermo RSLC pepmap100, 50cm reversed phase nano column at a flow rate of 300 nL min^{-1}. The eluent was nebulized and ionized using the Thermo nano electrospray source. Peptides were selected for MS/MS analysis in full MS/dd-MS2 (TopN) mode with the following parameter settings: TopN 10, resolution 17500, MS/MS AGC target 1e5, 60ms Max IT, NCE 27 and 3 m z^{-1} isolation window. Underfill ratio was at 10% and dynamic exclusion was set to 15 seconds. Data from the LC-MS/MS run was exported to Mascot generic file format using proteo wizard open source software and searched against an in-house curated database of PASK protein sequence and the SwissProt database using the MASCOT search engine (version 2.4, Matrix Science Inc., London, UK) with all taxonomy selected. The following search parameters were used: missed cleavages, 1; peptide mass tolerance, ± 20 ppm Da; peptide fragment tolerance, ± 20 mmu; peptide charge, 2+, 3+ and 4+; fixed modifications, carbamidomethyl; Variable modification, oxidation (Met).

Transmission Electron Microscopy (TEM). A suspension containing the PASKE particles was cast on Formvar-coated copper grids, followed by overnight air-drying. The grids were then washed with pure water to remove salt and allowed to air dry. TEM imaging was conducted on a CM120 BioTWIN instrument (Philips, Germany) operating at an acceleration voltage of 120 kV.

Near Infra-Red (NIR) Confocal Microscopy. The NIR confocal images were taken on a customized confocal microscope. A Nikon (Tokyo, Japan) A1R Plus confocal microscope was modified to include a NIR solid-state continuous wave (CW) laser (Obis 30mW, 730-nm, Coherent Inc., Santa Clara, USA). This was mounted on a separate laser board (Nikon LU3, equipped with a manual laser attenuator). An 80/20 beam splitter was used as the primary dichroic. The emitted NIR fluorescent signal was reflected by a custom filter cube (secondary dichroic Mirror 801LP [Semrock FF801-Di02-25x36], Band Pass filter 796/41 [Semrock FF01-796-41-25]) and collected with a standard PMT as supplied with a Nikon A1R Plus confocal microscope.

Zetasizer measurements. The hydrodynamic diameter, scattering light intensity, and zeta(ζ)-potential of MS@PASKE, PASKE, BSA and polyethylene glycol (PEG) particles were measured using a Zetasizer Nano ZS instrument (Malvern Instruments, Malvern) equipped with a He−Ne ion laser (λ = 633-nm) as an incident beam. For the dynamic light scattering (DLS) measurements, a particle dispersion in PB was placed in a micro cuvette (ZEN0040, Malvern Instruments). The photon correlation function was analyzed by the cumulant method to derive the diffusion coefficients (DC) of the particles. The obtained DC was converted into the hydrodynamic diameter using the Stokes−Einstein equation: $DH = kBT/3\pi\eta DC$ (kB: Boltzmann constant, T: absolute temperature, η: viscosity of the solvent). For the ζ-potential measurements, a particle dispersion in PB (700 μL) was placed into a folded capillary cell (DTS1070, Malvern Instruments). The ζ-potential was obtained from the electrophoretic mobility and by using the Smoluchowski equation: $\zeta = 4\pi\eta\nu.\varepsilon^{-1}$ (η: viscosity of the solvent, ν: electrophoretic mobility, ε: dielectric constant of the solvent).

Cell association assays. THP-1 cells (ATCC) and RAW 264.7 cells (ATCC) were cultivated in Roswell Park Memorial Institute (RPMI) 1640 medium (Sigma Aldrich) or Dulbecco's Modified

Eagle's Medium respectively (DMEM) (Sigma Aldrich) supplemented with 10% Fetal Calf Serum (FCS), 1% L- Glutamine, and 1% penicillin/streptomycin. Particles (5×10^6 mL^{-1}) were incubated at 37C with 10^5 cells mL^{-1} (50:1 ratio) in 48-cell culture well plate (Corning, Sigma-Aldrich). PASKE-Cy5, PEG-Cy5, BSA-Cy5 and MS@PASKE-Cy5 particles were incubated for 1, 6 and 24 hours in the corresponding cell media or a mixture of cell media and human plasma (3:2 ratio). Cells were harvested, washed twice in phosphate buffer saline (PBS) and analyzed by flow cytometry (LSRFortessa, BD Biosciences). Cells association was identified from the fluorescence signal resulting from Cy5 labelled particles and percentage of association was measured from 10,000 events. For imaging flow cytometry (Amnis, ImageStreamX, Merck Millipore), THP-1 cells were labelled with LysoTracker Blue DND-22 (0.3 nM, ThermoFisher Scientific) and lysosomes were identified in 405-nm excitation 457/45 bandpass channel, Cy5 labelled particles were detected in the 642-nm excitation 702/85 bandpass channel and the cell structure was observed in the bright field channel. For confocal microscopy observation (A1R+, Nikon), RAW 264.7 cells were labelled with LysoTracker Blue DND-22 (0.3 nM, Life Technologies) and lysosomes were observed in the 405-nm channel, cell membranes were stained with wheat germ agglutinin Alexa Fluor 488 conjugate (WGA-AF488, 10 μg mL^{-1}, Life Technologies) and observed in the 488-nm channel and Cy5 labelled particles were detected in the 640-nm channel.

Biodegradability assays. PASKE and PEG particle degradation in tissue lysosomal fraction was tested *in vitro*. Freshly harvested mouse spleen, liver, kidney and lung tissue was homogenized (Ultra-turrax T10basic, IKA) and the lysosomal fraction was isolated from 200 mg mL^{-1} of tissue following a procedure described elsewhere.[1] PASKE-Cy5 and PEG-Cy5 particles (2×10^6 mL^{-1}) were incubated at 37°C with 50 μL of lysosomal fraction in 200 μL acetate buffer (100 mM sodium acetate, 5 mM calcium chloride, 1.33 mM EDTA and 2 mM DTT, pH 5.5) or in 50 μg mL^{-1}

Trypsin-EDTA (Gibco). The concentration of particles was measured at the beginning of the incubation (t=0) and at 0.5, 1, 6 and 24 hours incubations by flow cytometry (LSRFortessa, BD Biosciences) counting Cy5 positive event in a fixed volume and the percentage of degradation was calculated from the ratio of the concentration at t=0. Mean percentage of degradation ± SD was plotted over time (n=4). Additionally, PASKE-Cy7 and PEG-Cy7 particles were incubated at 37°C with the lysosomal fraction in acetate buffer (pH 5.5) or in 50 μg mL^{-1} Trypsin-EDTA overnight and were analyzed with SDS gel electrophoresis. The gel was scanned using an Odyssey CLx Infrared Imaging System (LI-COR, Biosciences) and particles or degradation products were detected in the 800-nm channel. Non-degraded particles were too big not migrate and were detected on top of the gel whereas degradation products migrated through the gel and were detected at the bottom of the gel.

Functionalization of PASKE with SCE5 and Mut-scFv single-chain antibodies. Single-chain antibody (scFv) SCE5, specific for the activated glycoprotein complex IIb/IIIa (GPIIb/IIIa), Mut-scFv, the non-targeted version of the antibody and green fluorescent protein (GFP), all designed with a leucine, proline, glutamic acid, threonine and glycine tag (LPETG) at the C-terminus for Sortase A conjugation and the Sortase A enzyme were produced as previously described.[2] The glycine modified bicyclo[6.1.0]nonyne (G-PEG_3-BCN) Sortase substrate was prepared as previously described.[3] The scFv were then covalently attached to the PASKE particles *via* Sortase A bioconjugation and copper-free click chemistry (Figure S3 A), following previously established protocol.[4] Briefly, SCE5-LPETG, Mut-scFv-LPETG or GFP-LPETG (30 μM) were incubated 5 hours while shaking with Sortase A (90 μM) and G-PEG_3-BCN (90 μM) in 1 mL of Tris buffer (50 mM Tris(hydroxymethyl)aminomethane hydrochloride, 150 mM sodium chloride, 0.5 mM calcium chloride, pH 8). At the end of the reaction, the Sortase A enzyme, which has a His_8 tag at

the C terminus and the residual G-His_8 cleaved fragment were removed from the reaction with metal affinity resin beads (TALON). The modification of the scFv with the BCN group was confirmed by the addition of Cyanine7-azide dye and analysis by SDS gel electrophoresis scanned with an Odyssey CLx Infrared Imaging System (Figure S3 B and C). PASKE particles were functionalized with azide group (N_3) by incubation for 2 hours at room temperature under gentle mixing with N-hydroxysuccinimide-azide linker (N_3-PEG_8-NHS ester, Conju-probe) and washed by 5 min centrifugations at 6,000 g. SCE5-BCN, Mut-scFv-BCN or GFP-BCN were then mixed with PASKE-N_3 at a 2:1 molar ratio for 2 hours at room temperature under gentle mixing to enable a copper-free click reaction. An additional control group was obtained from non-modified PASKE particles incubated with GFP-BCN. PASKE-Cy5-N_3 and PASKE-Cy5 incubated with GFP-BCN were analyzed in flow cytometry (Figure S3 D) and in confocal microscopy (Figure S3 E) to verify successful conjugation of GFP-BCN detected in 488-nm channel to PASKE-Cy5-N_3 observed in 640-nm channel. PASKE-Cy5-SCE5, PASKE-Cy7-SCE5, PASKE-Cy5-Mut-scFv and PASKE-Cy7-Mut-scFv were then prepared following similar copper-free click procedure with PASKE-Cy5-N_3 or PASKE-Cy7-N_3 with SCE5-BCN or Mut-scFv-BCN.

Human blood and plasma preparation. The recruitment of participants and collection of blood specimens was approved by the Alfred Hospital Ethics Committee (Project 67/15). Signed informed consent was obtained prior to participation. Human blood was collected *via* venipuncture into tri-sodium citrate (3.2% w/v final). For plasma preparation, whole blood was centrifuged at 1,700 g for 15 minutes and plasma was collected from the supernatant and stored at -30 ^{o}C.

Flow chamber experiments. Microfluidic polydimethylsiloxane channels deposited on glass coverslip micro were incubated with bovine type 1 collagen (250 µg mL^{-1} in 10 mM acetic acid) for 30 minutes and then perfused with anticoagulated human whole blood labelled with 3,30-

dihexyloxacarbocyanine iodide ($DiOC_6$, 0.5 ug mL^{-1}) for 3 minutes to allow platelets to adhere to the collagen fibers and form micro-aggregates. PASKE-Cy5-anti-GPIIb/IIIa-scFv and PASKE-Cy5-Mut-scFv particles were flown over the top of the microthrombi at a shear rate fixed at 300 s^{-1} for 3 minutes. Microthrombi were observed with an inverted confocal microscope (A1R+, Nikon) in the 488-nm channel and PASKE-Cy5 particles in the 640-nm channel. Time-lapse Z-stack acquisitions were performed with a fast piezo nanopositioning system (Nano-Drive, Mad City Labs Inc.) over the first minute and then a range of images were taken along the flow channels for quantification. The amount of microthrombi was measured in the 488-nm channel images with Image J (NIH, USA) and expressed as the area of surface coverage (in mm^2). The PASKE-Cy5-anti-GPIIb/IIIa-scFv or PASKE-Cy5-Mut-scFv adherent to the micro thrombi were counted in the 640-nm channel images. Results are presented as mean values of particles per mm^2 of thrombi ± SD (n=17).

Blood clearance. Mice were anaesthetized and PASKE-Cy5, PEG-Cy5, BSA-Cy5 and MS@PASKE-Cy5 particles were injected intravenously at a dose of 10^6 g^{-1}. Drops of 5 µL of blood were harvested from the venous circulation at 2.5, 5, 10, 30 and 60 minutes post-injection and sampled in 200 µL 10 mM PB buffer. Samples to determine the injected dose were prepared by diluting injected suspensions at 10^6 in 60 µL (total blood volume was approximated at 6% of the body weight) then sampling this dilution 5 µL into 200 µL. Particle concentrations were determined by flow cytometry (LSRFortessa, BD Biosciences) counting Cy5 positive event in a fixed volume and percentage from the number of particles counted in the injected dose samples were calculated. Mean percentage of injected dose ± SD were plotted over time post-injection with nonlinear fit (n=4).

Liver and spleen cell analysis. Mice were anaesthetized and PASKE-Cy5, PEG-Cy5 and MS@PASKE-Cy5 particles were injected intravenously at a dose of 10^6 g^{-1}. At 3 hours post-injection, mice were culled, slowly perfused with warm PBS buffer and spleen and liver tissue was harvested. The protocol for spleen and liver cell suspensions preparation and subtype identification by flow cytometry was adapted from a method described elsewhere.[5, 6] Briefly, spleen tissue was gently dissociated into a single cell suspension using a 40 μm cell strainer, and divided into 3 suspensions labelled as follows: Suspension 1 was stained with a B220-FITC antibody to label B-cells and CD4/CD8-BV605 to label T-cells; suspension 2 was stained with CD41-FITC to label platelets and megakaryocytes and Ter119-PE to label red blood cells; suspension 3 was stained with F4/80-PE to label macrophages, Ly6C-BV605 to label monocytes and Ly6G-APC/Cy7 to label granulocytes. The gating strategy to identify cell subtypes in the spleen is presented in Figure S5. The liver tissue was incubated at 100 mg mL^{-1} with type IV collagenase (0.1%, Gibco), gently teased with forceps until a homogenous mixture was obtained, filtered through a 40 μm cell strainer and suspensions were labelled as follows; B220-FITC antibody to label B-cells, CD4/CD8-BV605 to label T-cells, CD31-PerCP/Cy5.5 to label endothelial cells, F4/80 PE and Mac1-V450 to identify inflammatory monocyte-derived (IMD) macrophages and Kupffer cells and the hepatocytes were identified as the non-labelled remaining cells. The gating strategy to identify cell subtypes in the liver is presented in Figure S6. The amount of Cy5 labelled particles in each cell subtype population was counted in the R-670/14 channel, expressed as the percentage of the amount of the cell subtype and presented as mean values ± SD (n=3).

Histology. Mice were anaesthetized and PASKE-Cy5, PEG-Cy5 and MS@PASKE-Cy5 particles were injected intravenously at a dose of 10^6 g^{-1}. At 30 minutes and 24 hours post-injection, mice were culled, slowly perfused with warm PBS buffer, the spleen and liver tissue was harvested and

fixed in 10% neutral buffered formalin for 24 hours. Processing to paraffin wax was carried out in a tissue processor (Leica Peloris II) and tissues were embedded in paraffin media. 4 μm thick paraffin sections of liver and spleen were prepared using a microtome (Leica RM2235 rotary), mounted on Superfrost Plus slides and allowed to dry prior to dewaxing and staining. Section were stained with wheat germ agglutinin Alexa Fluor 488 conjugate (WGA-AF488, 10 μg mL^{-1}, Life Technologies) to observe cell membrane in the 488-nm channel, with Hoechst 33342 (0.1 mg mL^{-1}, Life Technologies) to observe cell nuclei in 405-nm channel and Cy5 labelled particles were detected in the 640-nm channel.

Transmigration of PASKE particles across a human umbilical vein endothelial cell monolayer into collagen gels. PASKE-Cy5 particles were incubated at 10^6 particles mL^{-1} for 24 h on type I fibrous collagen gels overlaid with a tumour necrosis factor (TNF)-activated or non-activated primary human umbilical vein endothelial cell (HUVEC) monolayer prepared as previously described.[7] Following transmigration, gels were washed once with phosphate buffer saline (PBS) and fixed overnight in 2% formaldehyde. The next day, gels were stained with Hoechst 33342 (0.1 mg mL^{-1}, Life Technologies) for 30 mins, washed once with PBS and stained with wheat germ agglutinin Alexa Fluor 488 conjugate (WGA-AF488, 10 μg mL^{-1}, Life Technologies) for 20 mins. Gels were extracted and mounted on microscope slides as described elsewhere and analyzed by confocal microscopy (A1R+, Nikon).[7] Two 100 μm Z-stack observations were performed per gels from four gels per condition. Cy5 labelled particles localized within the collagen gel were counted in the 640-nm channel and expressed as mean number of particles per surface area of cell monolayer ± SD (n=8).

Statistical analysis. All results are expressed as mean values ± SD. Statistical analysis was performed with GraphPad Prism V7 (GraphPad Software). Cell association and tissue

biodistribution results were compared with two-way ANOVA with Tukey's multiple comparison post-tests. Flow chamber and particle migration data were compared with unpaired t-tests. A difference of $p<0.05$ was considered significant.

REFERENCES

1. Ohshita, T.; Hiroi, Y., Degradation of Serum Albumin by Rat Liver and Kidney Lysosomes. *J Nutr Sci Vitaminol (Tokyo)* **1998,** *44*, 641-653.
2. Ta, H. T.; Prabhu, S.; Leitner, E.; Jia, F.; von Elverfeldt, D.; Jackson, K. E.; Heidt, T.; Nair, A. K.; Pearce, H.; von zur Muhlen, C.; Wang, X.; Peter, K.; Hagemeyer, C. E., Enzymatic Single-Chain Antibody Tagging: A Universal Approach to Targeted Molecular Imaging and Cell Homing in Cardiovascular Disease. *Circ Res* **2011,** *109*, 365-373.
3. Alt, K.; Paterson, B. M.; Westein, E.; Rudd, S. E.; Poniger, S. S.; Jagdale, S.; Ardipradja, K.; Connell, T. U.; Krippner, G. Y.; Nair, A. K.; Wang, X.; Tochon-Danguy, H. J.; Donnelly, P. S.; Peter, K.; Hagemeyer, C. E., A Versatile Approach for the Site-Specific Modification of Recombinant Antibodies Using a Combination of Enzyme-Mediated Bioconjugation and Click Chemistry. *Angew Chem Int Ed Engl* **2015,** *54*, 7515-7519.
4. Hagemeyer, C. E.; Alt, K.; Johnston, A. P.; Such, G. K.; Ta, H. T.; Leung, M. K.; Prabhu, S.; Wang, X.; Caruso, F.; Peter, K., Particle Generation, Functionalization and Sortase A-Mediated Modification with Targeting of Single-Chain Antibodies for Diagnostic and Therapeutic Use. *Nat Protoc* **2015,** *10*, 90-105.
5. Rose, S.; Misharin, A.; Perlman, H., A Novel Ly6C/Ly6G-Based Strategy to Analyze the Mouse Splenic Myeloid Compartment. *Cytometry A* **2012,** *81*, 343-350.
6. Tsoi, K. M.; MacParland, S. A.; Ma, X. Z.; Spetzler, V. N.; Echeverri, J.; Ouyang, B.; Fadel, S. M.; Sykes, E. A.; Goldaracena, N.; Kaths, J. M. *et al.* Mechanism of Hard-Nanomaterial Clearance by the Liver. *Nat Mater* **2016,** *15*, 1212-1221.
7. Angelovich, T. A.; Hearps, A. C.; Maisa, A.; Kelesidis, T.; Jaworowski, A., Quantification of Monocyte Transmigration and Foam Cell Formation from Individuals with Chronic Inflammatory Conditions. *J Vis Exp* **2017,** *128*, e56293.

Table S1. Physicochemical Properties of MS@PASKE, PASKE, PEG and BSA particles

Particles	Size[a,b] (nm)	PDI[a]	ζ-potential[a] (mV)	Cell association	
				media	plasma
MS@PASKE	1213	0.016	-37 ± 6	+++	+++
PASKE	731 ± 6	0.353 ± 0.057	-9 ± 4	-	+
PEG	1066 ± 457[c]	-	-9 ± 3	-	-
BSA	671 ± 20	0.085 ± 0.033	-39 ± 4	+++	+++

a) Determined in phosphate buffer (pH 7.4, 10 mM). The results are expressed as mean ± standard deviation; b) Size denotes hydrodynamic diameter measured by diffracted light scattering except for PEG; c) The approximate size of the PEG particles was measured from confocal microscope images using an image analysis software (Image J); d) +++ strong association, + slow association, - low association

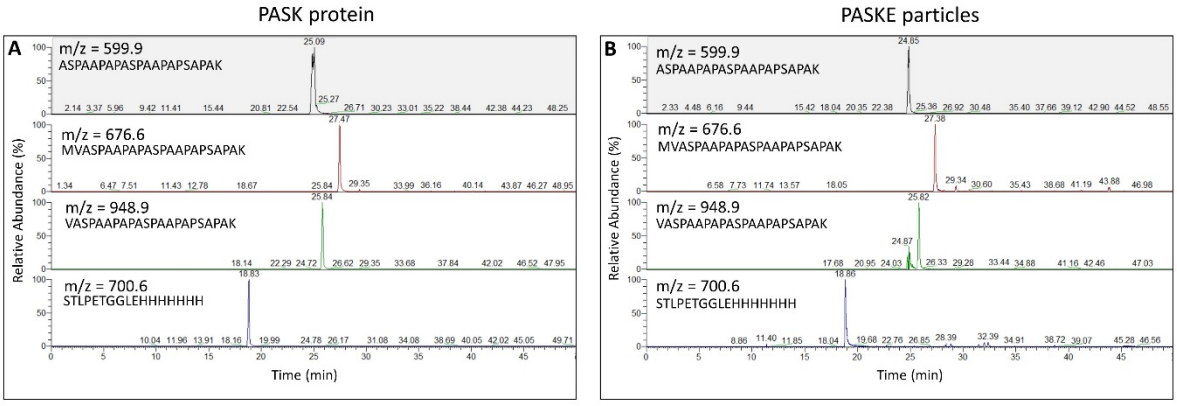

Figure S1: Ion chromatogram from liquid chromatography-mass spectrometry analysis of trypsin-digested PASK protein (**A**) and PASKE particles (**B**). The different peak corresponding to the 4 cleavage products ASPAAPAPASPAAPAPSAPAK, MVASPAAPAPASPAAPAPSAPAK, VASPAAPAPASPAAPAPSAPAK and STLPETGGLEHHHHHHHH were extracted at their corresponding mass to charge ratio. Data were exported and searched against an in-house curated database of PASK protein sequence and the SwissProt database using the MASCOT search engine;

matching scores of 1.87 10^4 and 1.22 10^4 were obtained for PASK protein and PASKE particles, respectively.

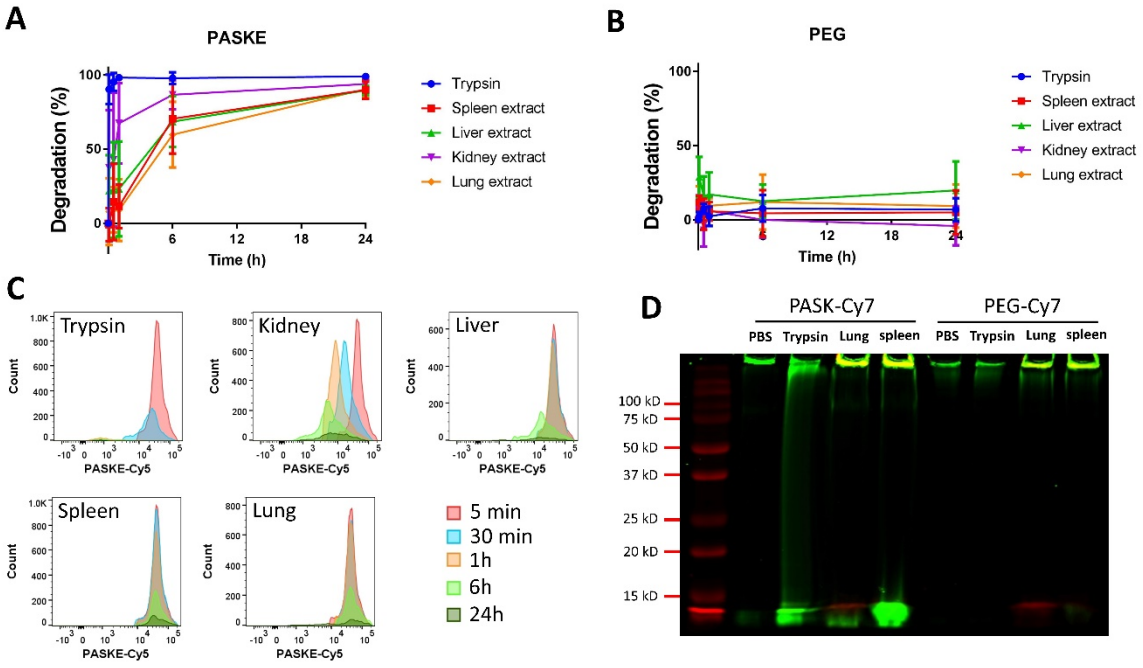

Figure S2: *In vitro* degradability of PASKE-Cy5 (**A**) and PEG-Cy5 (**B**) particles with lysosomal extract in acetate buffer (pH 5.5) or in 50 µg mL^{-1} Trypsin-EDTA over 24h as measured by flow cytometry. Mean percentage of degradation ± SD (n=4). (**C**) Overlay of flow cytometry sensograms obtained with PASKE-Cy5 incubated in Trypsin or in the lysosomal extract from mice kidney, liver, spleen or lung. (**D**) Degradability of PASKE-Cy7 or PEG-Cy7 in PBS, trypsin, lung or spleen lysosomal extract measured by sodium dodecyl sulfate (SDS) gel electrophoresis scanned with an Infrared Imaging System (Odyssey, LI-COR). Non-degraded particles were too big to migrate and were detected on top of the gel whereas degradation products migrated through the gel and were detected at the bottom of the gel.

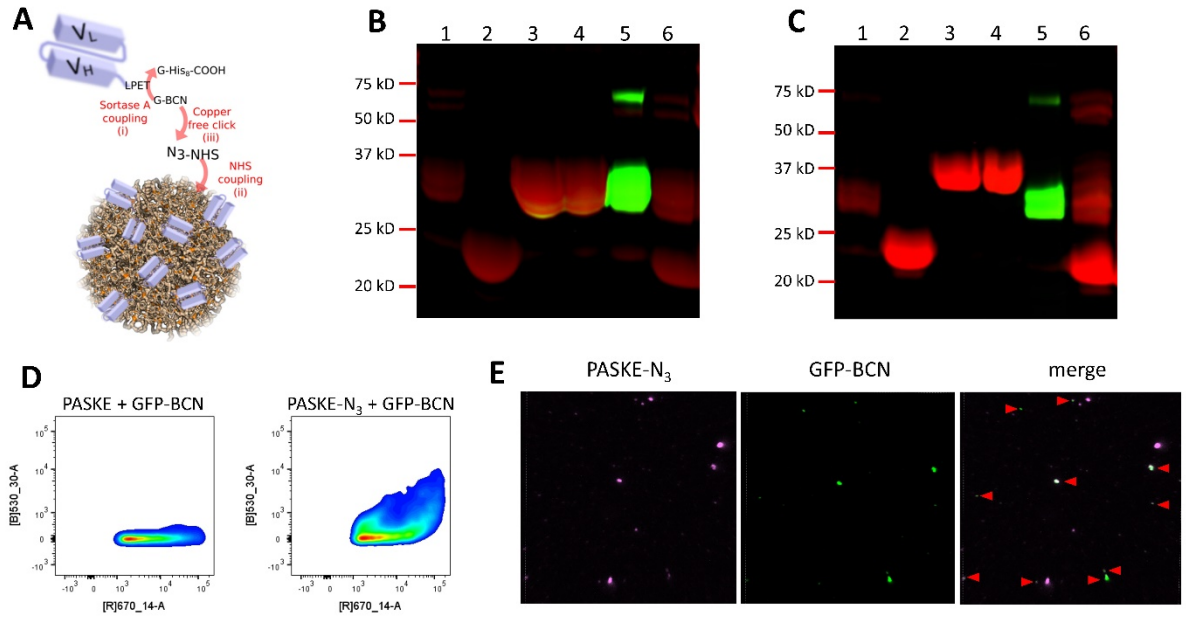

Figure S3: Functionalization of PASKE particles with single-chain antibodies using Sortase A conjugation coupled to copper-free click chemistry. (**A**) Scheme of the different step involved in the labelling; (i) the single-chain antibody is site-specifically modified with a C terminal bicyclo[6.1.0]nonyne (BCN) group *via* Sortase A conjugation, (ii) the remaining free primary amine groups from the lysines residues of PASKE particles are labelled with N-hydroxysuccinimide-azide linker (N_3-PEG_8-NHS) and (iii) BCN modified single-chain antibodies are attached on the surface of the PASKE-N_3 particles by copper-free click chemistry. Sortase conjugation of anti-GPIIb/IIIa-scFv (**B**) and Mut-scFv (**C**) single-chain antibodies was verified by Coomassie-stained sodium dodecyl sulfate (SDS) gel electrophoresis scanned with an Infrared Imaging System (Odyssey, LI-COR). Cyanine7-azide (N_3-Cy7) was used to confirm the presence of BCN group in the 800-nm channel (shown in green). Lanes for B; 1: anti-GPIIb/IIIa-scFv-BCN, 2: Sortase, 3: anti-GPIIb/IIIa-scFv, 4: anti-GPIIb/IIIa-scFv + Cyanine7-azide (N_3-Cy7), 5: anti-GPIIb/IIIa-scFv-BCN + N_3-Cy7, 6: anti-GPIIb/IIIa-scFv-BCN + Sortase (before harvesting Sortase with TALON beads). Lanes for C; 1: Mut-scFv-BCN, 2: Sortase, 3: Mut-scFv, 4: Mut-

scFv + N_3-Cy7, 5: Mut-scFv-BCN + N_3-Cy7, 6: Mut-scFv-BCN + Sortase (before harvesting Sortase with TALON beads). The success of the click conjugation on the surface of PASKE-Cy5 labelled with N_3-PEG_8-NHS (PASKE-Cy5-N_3) was then verified with the addition of green fluorescent protein functionalized with BCN group (GFP-BCN). The signal detected on the particles in the 488-nm channel indicated successful click conjugation. (**D**) Flow cytometry analysis of bare PASKE *versus* PASKE-N_3 incubated with GFP-BCN. (**E**) Confocal microscopy of PASKE-N_3-Cy5 particles shown in pink in the 640-nm channel and GFP-BCN signal shown in green in the 488-nm channel.

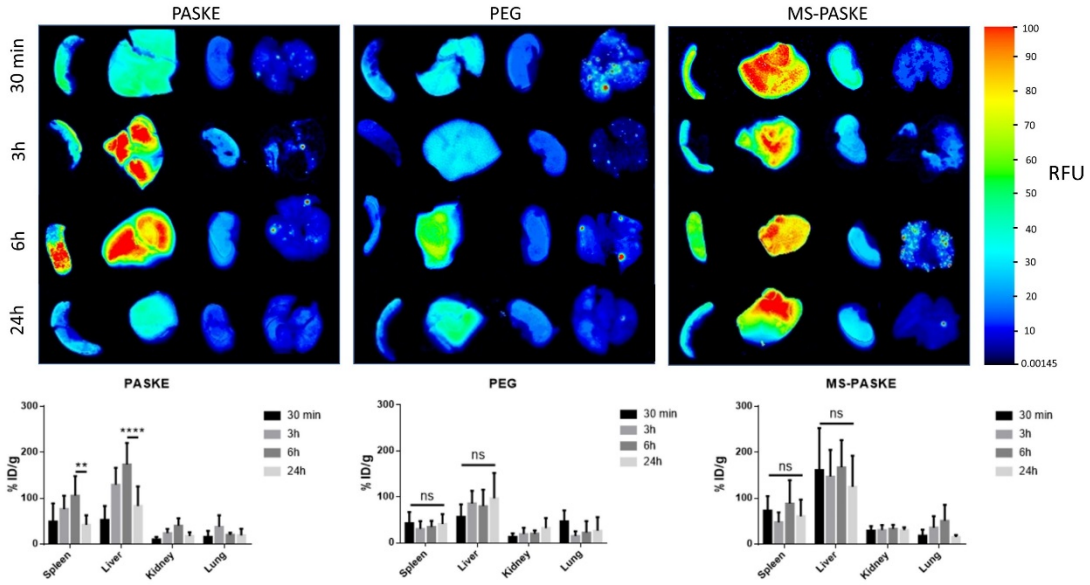

Figure S4: Tissue biodistribution study of PASKE, PEG and MS@PASKE particles labelled with Cyannine7 NHS ester. Animals were sacrificed at 30 min, 3h, 6h or 24h after intravenous injection, slowly perfused with saline, tissues of interest (the spleen, a part of the liver, the left kidney and the lung) were harvested and scanned using an Odyssey Infrared Imaging System. Representative scans showing the relative fluorescence intensity measured in the 800-nm channel are shown. The mean percentage of injected dose per gram of tissue values are presented as the mean ± standard deviation (n=4, two-way ANOVA, ****$p<0.0001$, **$p<0.01$, ns: non-significant).

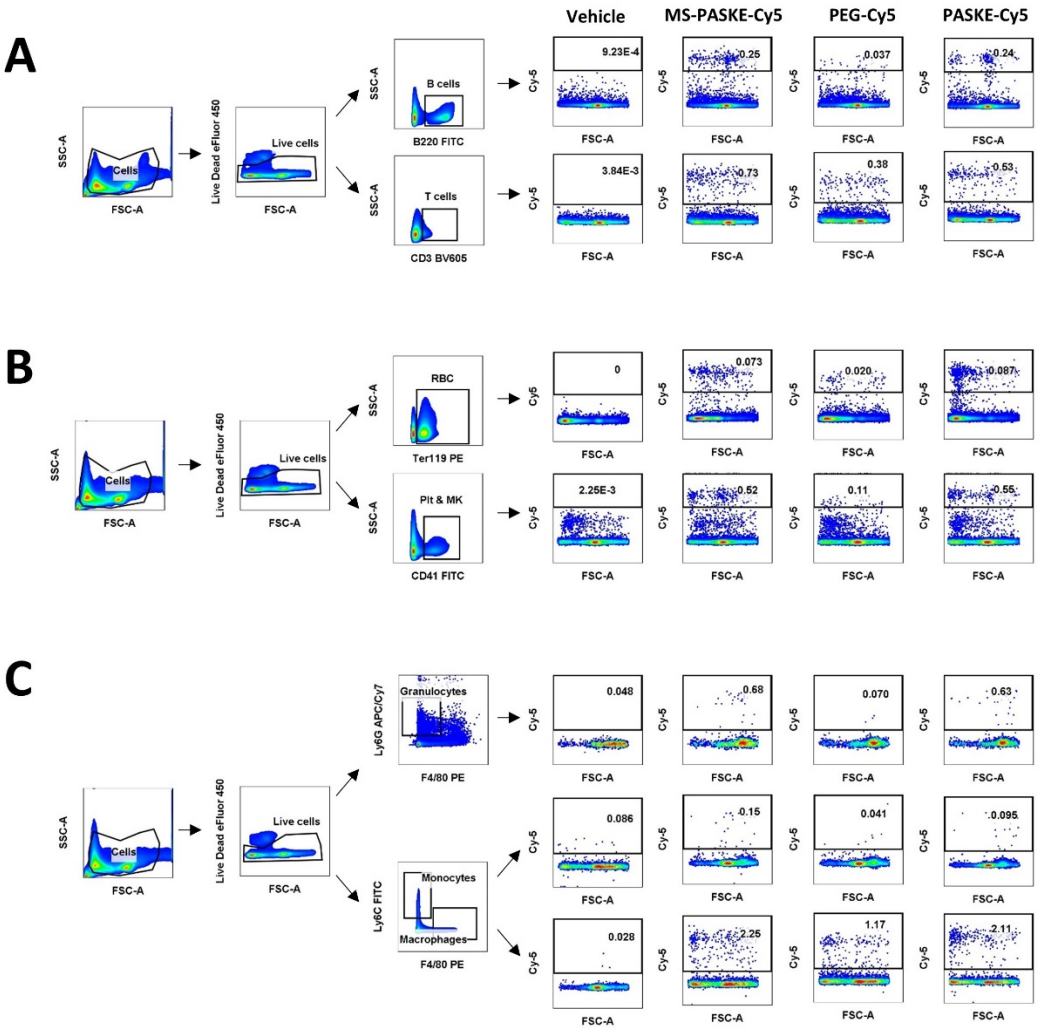

Figure S5: Gating strategy for spleen cell suspension analysis. (**A**) Suspension 1 stained with a B220-FITC antibody to label B-cells and CD4/CD8-BV605 to label T-cells. (**B**) suspension 2 stained with CD41-FITC to label platelets and megakaryocytes and Ter119-PE to label red blood cells. (**C**) suspension 3 stained with F4/80-PE to label macrophage, Ly6C-BV605 to label monocytes and Ly6G-APC/Cy7 to label granulocytes.

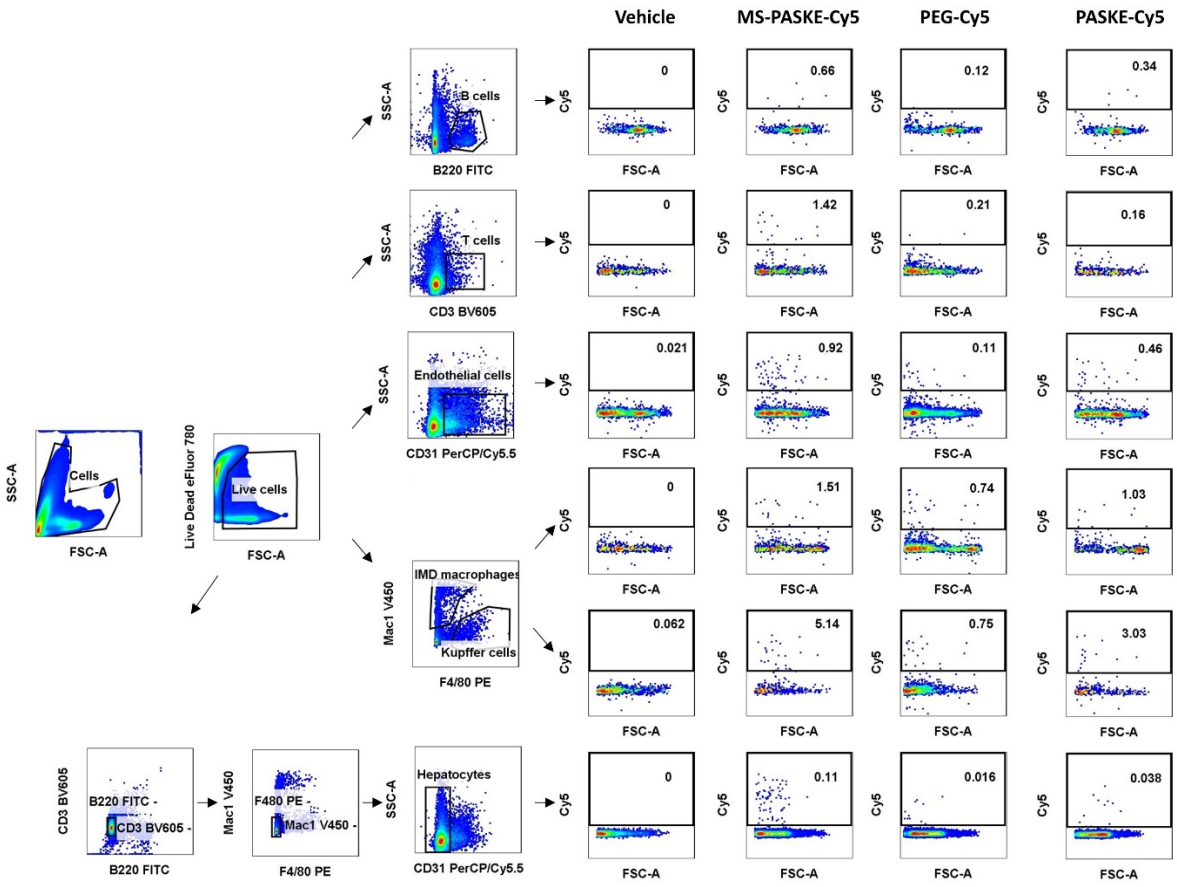

Figure S6: Gating strategy for liver cell suspension analysis. B-cells were labelled with a B220-FITC antibody, T-cells were labelled with CD4/CD8-BV605, endothelial cells were labelled CD31-PerCP/Cy5.5, F4/80 PE and Mac1-V450 were added to identify inflammatory monocyte-derived (IMD) macrophages and Kupffer cells. Hepatocytes were identified as the non-labelled remaining cells.

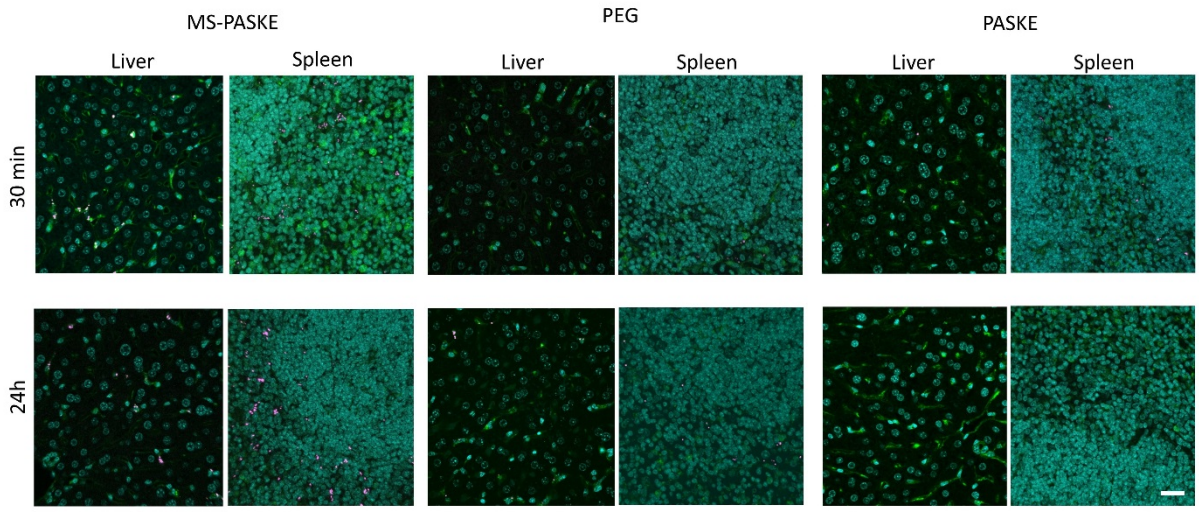

Figure S7: Histology observation of liver and spleen harvested at 30 min or 24h after injection of MS@PASKE-Cy5, PEG-Cy5 or PASKE-Cy5. Cell membrane and nuclei are stained with Alexa Fluor 488-conjugated wheat germ agglutinin (WGA-488, green) and Hoechst 33342 (cyan), respectively. Scale bar is 50 μm.

Author/s:
Bonnard, T; Jayapadman, A; Putri, JA; Cui, J; Ju, Y; Carmichael, C; Angelovich, TA; Cody, SH; French, S; Pascaud, K; Pearce, HA; Jagdale, S; Caruso, F; Hagemeyer, CE

Title:
Low-Fouling and Biodegradable Protein-Based Particles for Thrombus Imaging

Date:
2018-07-01

Citation:
Bonnard, T., Jayapadman, A., Putri, J. A., Cui, J., Ju, Y., Carmichael, C., Angelovich, T. A., Cody, S. H., French, S., Pascaud, K., Pearce, H. A., Jagdale, S., Caruso, F. & Hagemeyer, C. E. (2018). Low-Fouling and Biodegradable Protein-Based Particles for Thrombus Imaging. ACS NANO, 12 (7), pp.6988-6996. https://doi.org/10.1021/acsnano.8b02588.